MATERIALS CHEMISTRY FRONTIERS

REVIEW

View Article Online
View Journal | View Issue

Cite this: *Mater. Chem. Front.*, 2024, **8**, 1171

Recent advances in metal–organic frameworks for water absorption and their applications

Lu Cheng,† Yu Dang,† Yu Wang * and Kai-Jie Chen *

Potable water and energy shortage have become global issues. With the limited water adsorption performance and regeneration conditions of traditional water adsorbents, innovation in water adsorbents has significant practical implications. Due to the abundant varieties of adsorption sites and their adjustable pore structures, metal–organic frameworks (MOFs) are considered promising water adsorbents with tailorable regeneration conditions, controllable absorption humidity range, and superior water capacity. Herein, we combed through the development of water-uptake MOFs. Their water absorption mechanisms and strategies are summarized through analysis of typical examples. In addition, the recent advances of MOFs focused on atmospheric water harvesting, indoor humidity control, adsorption-driven heat pumps, and industrial chemical dehydration are reviewed. Finally, the possible challenges in the evolving prospects are predicted and the corresponding solutions are proposed.

Received 29th April 2023,
Accepted 28th November 2023

DOI: 10.1039/d3qm00484h

rsc.li/frontiers-materials

1. Introduction

Water is the most important survival resource for human beings. Although approximately 1.386 billion cubic kilometers of water exist on Earth, only about 0.0075% of the water can be directly used.[1] Furthermore, the unequal geographical and temporal distribution of freshwater resources, such as water resources being severely scarce in deserts and some inland areas, render efficient water collection in these regions particularly crucial.[2] As the atmosphere contains up to 12.9×10^9 million tons of water, the water scarcity issue in arid areas can be alleviated by collecting moisture from the atmosphere.[3] In addition, water is an excellent adsorbate for adsorption heat pumps and refrigeration systems as it is one of the cleanest natural energy sources with a high enthalpy of evaporation (40.7 kJ mol^{-1}).[4] Therefore, finding suitable water adsorbents is an effective alternative to solve water harvesting and energy conversion problems. Meanwhile, water adsorbents are widely applied in chemical dehydration,[5,6] indoor humidity maintenance,[7,8] food preservation[9] and other fields, and play an important role in many aspects of industrial production and daily life.

Traditional desiccants include zeolites, silica, metal chlorides, and metal oxides. Specifically, zeolites loaded with Na^+, K^+,

Key Laboratory of Special Functional and Smart Polymer Materials of Ministry of Industry and Information Technology, Xi'an Key Laboratory of Functional Organic Porous Materials, School of Chemistry and Chemical Engineering, Northwestern Polytechnical University, Xi'an, Shaanxi 710072, China.
E-mail: wychem@nwpu.edu.cn, ckjiscon@nwpu.edu.cn
† These authors contributed equally to this work.

Lu Cheng

Lu Cheng is currently a postgraduate student at Northwestern Polytechnical University under the supervision of Prof. Kai-Jie Chen and Dr Yu Wang. Her research focuses on the gas absorption and separation of MOFs.

Yu Dang

Yu Dang is pursuing a PhD at Northwestern Polytechnical University, supervised by Prof. Kai-Jie Chen. Her research focuses on the design and synthesis of high-performance MOFs for gas separation and absorption.

and Ca^{2+} ions can be used as high-temperature adsorbents due to their strong affinity and adsorption heat (3000–4500 kJ kg^{-1}).[10] However, the desorption temperature of zeolites needs to reach *ca.* 250–300 °C owing to the strong affinity, which is unfavourable for regeneration. Silica gels, composed of amorphous silica networks, characterized with high stability, can encapsulate water molecules relying on active silanol groups on the surface and inside the pores.[11] Although the regeneration temperature of silica gel can be adjusted by the pore polarity,[12] silica without being compounded with other adsorbents typically demonstrates low water uptake led by their relatively small surface area.[13] Chemical adsorbents, such as metal chloride and metal oxides, generally achieve water absorption through chemical reactions or by forming complexes but it is unrecoverable due to the irreversible chemical interactions.[14]

Given the significance of water adsorbents, there is great potential for the development of water adsorption materials that can satisfy the specific requirements of water absorption performance and regeneration conditions. Metal–organic frameworks (MOFs) are long-range ordered organic–inorganic hybrid porous materials with adaptable pore size and chemistry based on the features of metal ions and ligands.[22] Due to the essential attributes of ordered crystalline structure, tailorable hydrophilicity and adjustable pore size,[23,24] MOFs have been implemented extensively in gas separation,[25–27] catalysis,[28–30] and sensing.[31,32] They also have great application prospects in water adsorption with the advantages of tailorable regeneration temperature, controllable absorption humidity range and superior water capacity[33] (Fig. 1).

In this review, we will introduce the design strategies of MOFs for water absorption and discuss the representative application of water absorption MOFs in detail including atmospheric water harvesting, indoor humidity control, adsorption-driven heat pump and industrial chemicals dehydration (Fig. 2).

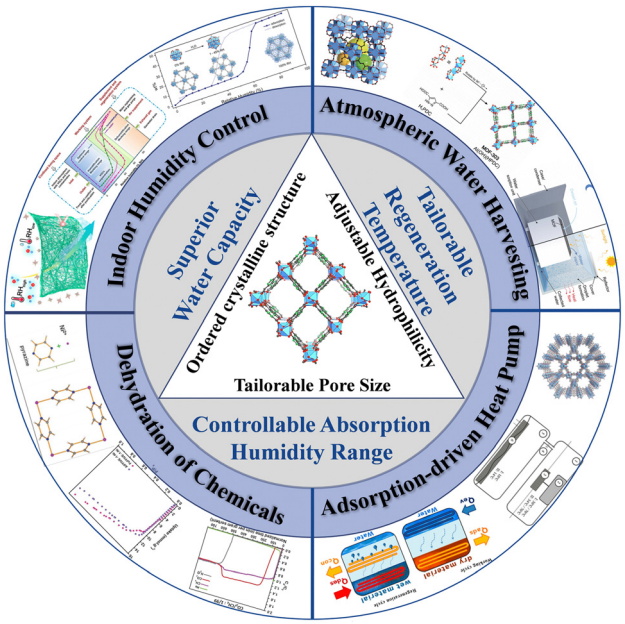

Fig. 1 Schematic illustration of the structure, superiority and applications of water absorption MOFs. Reprinted with permissions from ref. 2, 8 and 15–21. Copyright 2017, American Association for the Advancement of Science. Copyright 2018, American Association for the Advancement of Science. Copyright 2018, Springer Nature. Copyright 2017, Wiley-VCH Verlag GmbH & Co. KGaA, Weinheim. Copyright 2019, American Chemical Society. Copyright 2017, The American Association for the Advancement of Science. Copyright 2020, American Chemical Society. Copyright 2021 Wiley-VCH GmbH. Copyright 2018, Wiley-VCH Verlag GmbH & Co.

2. Regulation strategies for water adsorption by MOFs

2.1 Classification and water absorption behavior of MOFs

Adsorption isotherms evaluate the water absorption performance of an adsorbent. The affinity of a material for water

Yu Wang

Dr. Yu Wang received his BSc and MEng from South China University of Technology and Lanzhou University in 2012 and 2015, respectively. He then earned his PhD under the supervision of Prof. Jie-Peng Zhang from Sun Yat-Sen University in 2019. From 2019 to 2021, he worked as a postdoctoral researcher at AIST-Kyoto University ChEM-OIL in Kyoto University under the supervision of Prof. Qiang Xu. He is currently an associate professor at Northwestern Polytechnical University. His research interest is on the design/modification of porous coordination polymers and their applications in gas separation and catalysis.

Kai-Jie Chen

Prof. Kai-Jie Chen finished his undergraduate study in 2008 at Zhengzhou University, and earned his PhD under the supervision of Prof. Xiao-Ming Chen from Sun Yat-Sen University in 2013. Then he conducted postdoctoral research in Prof. Michael J. Zaworotko's group at the University of Limerick from 2014 to 2018. After that, he joined Northwestern Polytechnical University in 2018 as a full professor. His current research interests are focused on crystal engineering of porous coordination polymers for application of related gas separation and energy conversion.

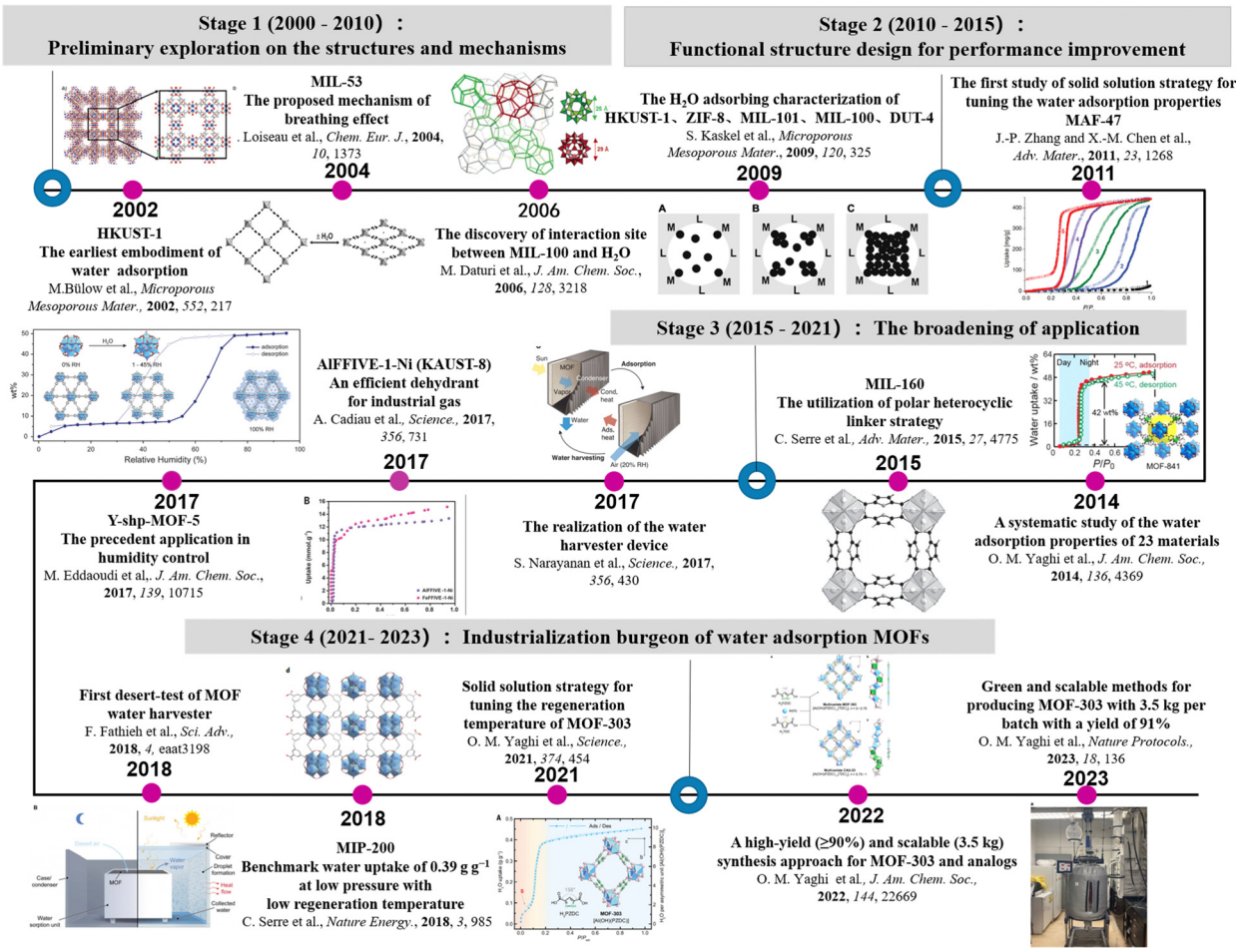

Fig. 2 The timeline of MOF utilization in water absorption. Reprinted with permissions from ref. 2, 15–17, 20 and 34–43. Copyright 2013, American Chemical Society. Copyright 2004, Wiley-VCH Verlag GmbH & Co. KGaA, Weinheim. Copyright 2006, American Chemical Society. Copyright 2009, Elsevier Inc. Copyright 2011, Wiley-VCH Verlag GmbH & Co. KGaA, Weinheim Copyright 2014, American Chemical Society. Copyright 2015, Wiley-VCH Verlag GmbH & Co. KGaA, Weinheim. Copyright 2017, American Association for the Advancement of Science. Copyright 2017, The American Association for the Advancement of Science. Copyright 2018, Wiley-VCH Verlag GmbH & Co. KGaA, Weinheim. Copyright 2018, American Association for the Advancement of Science. Copyright 2018, Springer Nature. Copyright 2021, The American Association for the Advancement of Science. Copyright 2022, American Chemical Society. Copyright 2022, Springer Nature Limited.

molecules and the adsorption process can be anticipated by analyzing the form of the isotherms and the position of the inflection point, which is vital to provide alternatives as water adsorbents in different application domains. As shown in Fig. 3, IUPAC suggests that physical adsorption isotherms can be divided into six types. Types I, II and III belong to reversible adsorption, with no hysteresis between adsorption and desorption.[44]

(1) Microporous (pore width < 2 nm) adsorbents possess type I adsorption isotherms.[32] In general, MOFs with open metal sites (OMSs, *e.g.* MOF-74,[45] HKUST-1[46]) or microporous MOFs with strongly hydrophilic pore channels (*e.g.* CAU-10-NH_2[47]), typically exhibit type I adsorption isotherms due to their strong affinity.

(2) MOFs absorbing water through a monolayer–multilayer adsorption mechanism usually show type II adsorption isotherms. A portion of the microporous MOF initially absorbs water using unsaturated metals or polarity sites on ligands, and then the primarily adsorbed water molecules continuously attract water to form water clusters or networks through hydrogen bonds, ultimately leading to pore filling. The adsorption of water *via* monolayer adsorption is relatively low and then rises abruptly due to multilayer adsorption with an obvious inflection point B. For instance, water molecules prefer to adhere to the μ_3-OH located on the Zr-SBU in MOF-801 under low relative pressure,[39] whereas in MOF-303, they prefer to adapt to the hydroxyl group of the ligand.[41] All these primary adsorptions serve as binding sites for additional hydrogen bonding and water cluster formation.

(3) Since the interaction between adsorbent and adsorbate is relatively low, water molecules prefer surfaces with a high adsorption affinity, leading to the curve shown in type III isotherms.

(4) Type IV isotherms are generally found for mesoporous materials. At low relative pressures, the isotherms show a curve similar to type II, but the difference is that there is a desorption

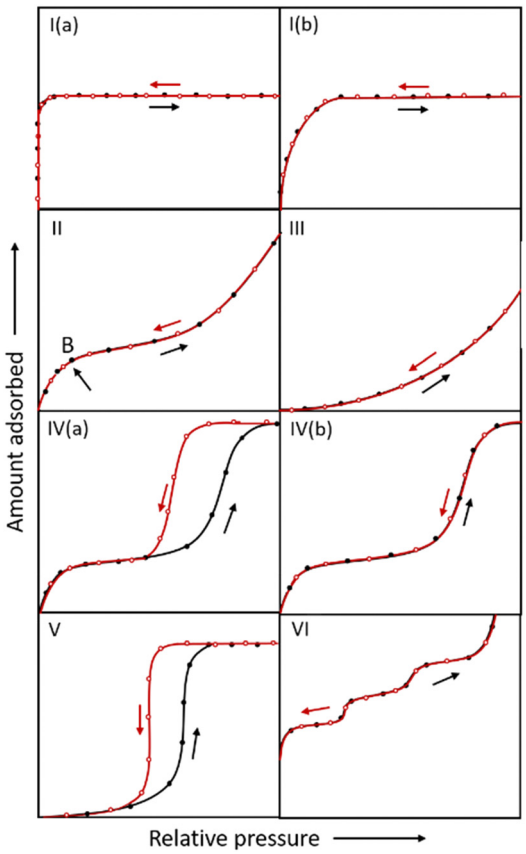

Fig. 3 IUPAC classification of adsorption isotherms. The black and red lines represent the adsorption and desorption curves, respectively.

hysteresis at the middle-pressure section for type IV(a) isotherms. The mesoporous adsorbents undergo monolayer–multilayer adsorption, with the pore wall serving as the primary adsorption site. When the pressure rises, the pore diameter expands until it approaches the critical diameter, at which stage capillary condensation occurs and the adsorption amount rises dramatically. At room temperature, the critical diameter for capillary condensation is 2.076 nm when the adsorbate is water.[48] Due to irreversible capillary condensation, which is regulated by the pore size of mesoporous materials, a hysteresis loop between adsorption and desorption exists. MIL-101, a typical mesoporous MOF with a high capacity for water absorption, undergoes capillary condensation at $P/P_0 \sim 0.4$. With two different-sized pores of 2.9 nm and 3.4 nm, water molecules first adsorb in the smaller cages before further filling in the larger cages, a phenomenon known as stepwise adsorption. The adsorption isotherm of MIL-101 roughly corresponds to type IV(a).[49]

When the pore size of mesoporous materials is smaller than the critical diameter of capillary condensation at the completion of monolayer adsorption, no capillary condensation occurs and the desorption curve is fully reversible. In the case of Co_2Cl_2(btdd), which has a pore size of 2.2 nm, monolayer adsorption is carried out firstly in the low relative pressure region and subsequently the pore size is reduced to 2 nm. Hence, pore filling occurs and is fully reversible, and the adsorption isotherm is represented as IV(b).[50]

(5) Microporous or mesoporous materials with hydrophobic pore channels generate type V adsorption isotherms, which are similar to type III in the low relative pressure region due to the weak adsorbent–adsorbate interaction at low pressures. When the relative pressure exceeds a particular value, a fast adsorptive uptake and a hysteresis loop exist due to the occurrence of irreversible phenomena such as capillary condensation.

(6) Materials with highly homogeneous non-porous surfaces result in type VI adsorption isotherms, which show a step-like appearance attributed to the sequential porous adsorption.

2.2 Water stability

Hydrolytic stability is the most important prerequisite for a water adsorbent. Although certain MOFs are unstable in the presence of water as they are assembled from relatively weak coordination bonds, numerous MOFs exhibit remarkable water stability due to their structural diversity and rational design.[51] A reasonable structural design of MOFs enables stability under strong acidic or alkaline conditions for complex working conditions.[52]

There are two pathways in MOF degradation in the presence of water: (i) hydrolysis and (ii) ligand–ligand substitution. During the hydrolysis process, the metal–ligand bond is attacked by the hydroxide anion and the proton dissociates from the water, forming the metal hydroxide and protonated ligand, as shown in eqn (1).[53]

$$\text{M–L} + \text{H}_2\text{O} \rightarrow \text{M–(OH)} + \text{LH} \quad (1)$$

As indicated in eqn (2), the ligand–ligand substitution process involves the insertion of water molecules into the metal–ligand bond, releasing the deprotonated ligand.

$$\text{M–L} + \text{H}_2\text{O} \rightarrow \text{M–(OH)}\cdots\text{LH} \quad (2)$$

The water hydrolysis stability of MOF is greatly influenced by the electronic effects of metal and the steric shielding effects of the linker.[54,55] In general, metals with strong electronic effects are more likely to establish strong metal–ligand bonds with ligands, and tightly connected linkers with strong shielding effects can effectively protect the coordination bonds to prevent water attack.

In accordance with the hard–soft acid–base theory, high-valent metal ions (hard acids) with a high charge density have a strong affinity for the carboxylic acid ligands (hard bases), forming strong coordination bonds. Consequently, the MOFs composed of hard acids and hard bases can offer ultra-high water stability. By way of illustration, MIL-100 (Al, Fe) composed of M^{3+} and benzene-1,3,5-tricarboxylic acid, can maintain excellent crystallinity and porosity after the adsorption at 40 °C and desorption at 140 °C for 40 cycles.[56] As a result of the high polarization of the coordination bond, MOFs constructed through soft acid and soft base, such as MAF-41 [Cu_2(fbdim)], may also offer exceptional water stability.[57]

2.3 Factors affecting water absorption performance in MOFs

The water absorption property of MOFs is mainly controlled by adjusting the pore size, pore chemistry and flexibility. The characteristics associated with the performance of traditional water adsorption MOFs are summarised in Table 1.

2.3.1 Pore size

(1) Absorption properties of microporous MOFs. The research on the water absorption performance of HKUST-1 ($[Cu_3(btc)_2(H_2O)_x]$, H_2btc = benzene-1,3,5-tricarboxylate) was published by Bülow and co-workers in 2002, as one of the earliest water adsorption studies of MOFs.[76] HKUST-1 contains OMS and two types of pore channels: hydrophilic large pores with pore sizes of 9 Å and hydrophobic small pores surrounded by benzene rings with pore sizes of 6 Å. The water adsorption isotherm of HKUST-1 is approximately type I (Fig. 4). At low relative pressures (P/P_0 = 0.1–0.3), water molecules preferentially adsorb near the OMS in the hydrophilic macropores to form coordination bonds, followed by pore filling, achieving a saturation adsorption of 0.45 g g^{-1} (45 wt%).[37] Due to the strong coordination between water molecules and open copper ions, water molecules cannot be completely desorbed in the low-pressure region. Particularly at 0% relative humidity, around 9% of the water molecules cannot be desorbed without heating (up to 200 °C).[46,77] HKUST-1 degraded severely when subjected to adsorption and desorption water cycling experiments, losing 53% of its capacity after 20 cycles.[78]

UiO-66 ($[Zr_6O_4(OH)_4(bdc)_{12}]$, H_2bdc = 1,4-benzenedicarboxylic) has been extensively explored due to its superior water and chemical stability. At low pressure, water molecules selectively interact with the m_3-OH of Zr clusters in UiO-66, which achieves less adsorption at this stage because of the comparatively hydrophobic pore surface. When the pressure reaches P/P_0 = 0.35, continuous pore filling occurs related to the formation of hydrogen bonds, resulting in a saturation adsorption capacity of almost 0.44 g g^{-1}. There is an irreversible hysteresis loop due to the limited flexibility of the backbone of the structure.[79,80] In consequence, the water adsorption of UiO-66 generates a type V isotherm.[81] With the same $Zr_6O_4(OH)_4(-CO_2)_{12}$ SBUs, MOF-801 $[Zr_6O_4(OH)_4(fumarate)_6]$ has similar absorption sites with UiO-66 (Fig. 5a–c). Due to the smaller sizes of cages, MOF-801 achieved a higher hydrophilicity and a tendency for the adsorption isotherm to move towards low relative pressure. In particular, at 25 °C, compared with UiO-66, MOF-801 embodies a steeper absorption at P/P_0 = 0.08 going towards a lower relative pressure and a lower saturation adsorption quantity of nearly 0.36 g g^{-1}, presenting a type II isotherm (Fig. 5d). Simultaneously, an increase in defects may enhance the hydrophilicity and specific surface area of MOF-801, resulting in a larger adsorption capacity of around 0.40 g g^{-1} and a propensity for isotherms to shift towards the low-pressure region.[39]

With the longer 2,6-naphthalic acid, the cage diameters of DUT-52 rise to 8.0 Å and 10.1 Å, which leads to lower hydrophilicity and less water uptake, hence necessitating a greater pressure for pore filling. At 25 °C, the pore-filling pressure for DUT-52 is P/P_0 = 0.4, which is larger than that of UiO-66. In conclusion, the pore size adjustment can alter the hydrophilicity of adsorbent, then influence its water absorption behaviors. With an increase in pore size, the stage of pore filling in a given topology often proceeds in the direction of increased pressure.[60]

CAU-10 ([Al(OH)(*m*-bdc)], *m*-H_2bdc = 1,3-benzenedicarboxylic acid) is composed of isophthalate and helical chains assembled by *cis* vertex-sharing octahedral AlO_6 units, with a square one-dimensional channel (*ca.* 5.6 Å).[82] CAU-10 features a steep absorption trend at $0.15 < P/P_0 < 0.20$, because of the small pore size of 5.6 Å and hydrophilic pore surface. Water molecules preferentially engage with the hydroxyl group linked to the metal center, followed by multi-adsorption occurring based on the initially adsorbed water, resulting in a saturation adsorption capacity of around 0.32 g g^{-1} at 25 °C.[16] Furthermore, CAU-10 can maintain its initial adsorption capacity after 700 cycles due to its stable one-dimensional chains formed by the Al–O bonds and negligible hysteresis loop.[62,83]

MIP-200 $[Zr_6(\mu_3\text{-}O)_4(\mu_3\text{-}OH)_4(mdip)_2(formate)_4]$, formed by a Zr_6 oxocluster and linked by tetracarboxylic acid ligand (3,3′,5,5′-tetracarboxydiphenylmet-hane, H_4mdip), contains two types of channel, 13 Å and 6.8 Å, respectively. Noticeably, at excessively low relative pressure (P/P_0 = 0.01), water molecules are preferentially encapsulated between two Zr_6 SBUs, interacting with the hydroxyl group and the metal center (Fig. 6a), yielding a strong zero-point heat of adsorption (70 kJ mol^{-1}). Thus, a surge of water adsorption at the initial relative pressure was observed, implying the high degree of hydrophilicity. As the relative pressure attained was P/P_0 = 0.1, the moisture content in the system was rationalized to pore filling. The majority of water was absorbed by MIP-200 at $P/P_0 < 0.25$, as indicated in Fig. 6b. At 30 °C and P/P_0 = 0.3, the equilibrium water uptake of 0.39 g g^{-1} is considerably higher than that of CAU-10 (0.30 g g^{-1}) and MOF-801 (0.28 g g^{-1}) (Fig. 6c). Most of the water molecules (25.1 wt%) can be removed below 65 °C, while more strongly bound water molecules (6.0 wt%) were released between 70 and 160 °C. As there is no hysteresis between the adsorption and desorption, the adsorption process was highly reversible with negligible energy loss (Fig. 6d).[17]

Y-shp-MOF-5 $[Y_9(\mu_3\text{-}O)_2(\mu_3\text{-}OH)_{12}(OH)_2(H_2O)_7(bteb)_3]$ contains trigonal one-dimensional channels with diameters of 12 Å, with bteb (bteb = 1,2,4,5-tetrakis(4-carboxyphenyl)benzene) serving as a ligand. At low relative pressure ($P/P_0 < 0.1$), water molecules are adsorbed on the open metal site and the bridging hydroxide ion by generating coordinate bonds and hydrogen bonds, respectively. Subsequently, the adsorbed molecules serve as secondary adsorption sites for additional water adsorption, after which the uptake reaches a platform due to the strong hydrophobicity of the ligand BTEB. Until the relative pressure approaches 0.5, the water molecules at the secondary adsorption sites are connected together by intermolecular hydrogen bonds to form superclusters, with rapid pore filling and a saturated adsorption quantity of 0.50 g g^{-1}. Therefore, additional energy input is required to dissociate the superclusters during the desorption process, resulting in a significant hysteresis loop between 30% and 70% relative humidity. Strong contact between the water

Table 1 Summary of reported MOF porous features and water adsorption properties measured at 25 °C (unless specified)

MOF	Pore volume/nm	Pore size/nm	S_{BET}/m^2 g^{-1}	α	Water adsorption capacity/g g^{-1}/cm^3 g^{-1}	Desorption temperature/°C	Cycling stability	Potential applications	Ref.
HKUST-1	0.62	0.9/0.6	1340	0.18	0.45/0.56	110	Unstable over 40% RH	Dehydrating under low RH	37
Ni-MOF-74	0.46	1.1	1040	0.02	0.40/0.50	110	5	Sea water desalination	39
Mg-MOF-74	0.53	1.1	1250	0.02	0.48/0.60	110	5	Sea water desalination	37
Al-fumarate	0.48	0.6/0.45	1021	0.25	0.47/0.59	65	4500	Heat exchanger	58
UiO-66	0.49	1.1/0.8	1290	0.3	0.44/0.55	80	5	Heat exchanger	39
UiO-66-NH_2	0.52	NR	1123	0.15	0.27/0.34	65	NR	Heat exchanger	59
UiO-66-NO_2	0.4	NR	792	0.15	0.40/0.50	65	NR	Heat exchanger	59
UiO-66-OH	0.44	0.83/0.66	1099	0.22	0.39/0.49	65	NR	Heat exchanger	60
UiO-66-N	0.57	0.81/0.73	1413	0.15	0.49/0.61	80	NR	Heat exchanger	60
DUT-52	0.66	1.01/0.8	2025	0.4	0.35/0.44	85	NR	Heat exchanger	60
UiO-67	0.90	2.16/1.09	1639	0.5	0.18/0.22	85	Poor stability	Heat exchanger	60
MOF-801	0.45	0.74/0.56/0.48	990	0.08	0.36/0.45	65	3000	Water harvesting at low RH, heat exchanger	39
MOF-841	0.53	0.92	1390	0.23	0.48/0.60	70	5	Exchanger	39
MOF-808	0.84	1.84/0.48	2060	0.30	0.60/0.75	60	5	Heat exchanger	39
DUT-67	0.60	1.66/0.74	1560	0.49	0.5/0.62	100	20	Heat exchanger	61
CAU-6	0.34	0.91	760	0.05	0.3/0.37	NR	5	Heat exchanger	39
CAU-10	0.27	0.56	525	0.15	0.35/0.44	70	700	Heat exchanger	62
CAU-10-NO_2	NR	NR	440	0.33	0.16/0.20	NR	NR	Heat exchanger	47
CAU-10-OH	NR	NR	NR	0.12	0.31/0.39	NR	NR	Heat exchanger	47
CAU-10-NH_2	NR	NR	NR	0.12	0.22/0.27	NR	NR	Heat exchanger	47
CAU-10-CH_3	NR	NR	NR	0.45	0.18/0.22	NR	NR	Heat exchanger	47
CAU-10-OCH_3	NR	NR	NR	0.26	0.09/0.11	NR	NR	Heat exchanger	47
MIL-160	0.398	0.5	1070	0.08	0.37/0.46	80	10	Water harvesting at low RH, heat exchanger	40
MIL-125	0.68	0.61	1510	0.38	0.30/0.37	150	NR	Heat exchanger	63
Al-MIL-53	0.51	n.d.	NR	0.30	0.09/0.11	NR	NR	Heat exchanger	64
Al-MIL-53-OH	NR	n.d.	NR	0.75	0.40/0.50	NR	NR	Heat exchanger	64
Al-MIL-53-NH_2	NR	n.d.	NR	0.02	0.09/0.11	NR	NR	Heat exchanger	64
Al-MIL-53-$(COOH)_2$	NR	n.d.	NR	0.30	0.13/0.16	NR	NR	Heat exchanger	65
MIP-200	0.4	1.3/0.68	1000	0.18	0.39/0.49 (30 °C)	70	50	Heat exchanger	17
Y-shp-MOF-5	0.63	1.2	1550	0.37	0.50/0.62	Room temperature under vacuum	200	Indoor humidity maintenance	7
MOF-303	0.5	0.94	1360	0.12	0.45/0.56	65	2000	Water harvesting at low RH	41
MOF-333	0.5	0.94	1280	0.23	0.44/0.55	55	2000	Water harvesting at low RH	41
ALP-MOF-1	NR	1.2/0.95	1900	0.80	0.59/0.73	75	NR	Heat exchanger	66
ALP-MOF-2	NR	1.2/0.95	1860	0.32	0.38/0.47	120	NR	Heat exchanger	66
MIL-100(Fe)	1	2.9/2.5	1917	0.26	0.8/1.0	140	40	Water harvesting at high RH	67
MIL-100(Al)	1.14	2.9/2.5	1814	0.26	0.5/0.62	140	40	Water harvesting at high RH	56
MIL-100(Cr)	1.14	2.9/2.5	1848	0.26	0.8/1.0	140	40	Water harvesting at high RH	67
MIL-101	1.58	3.4/2.9	3124	0.4	1.4/1.74	140	40	Water harvesting at high RH	49
MIL-101-NH_2	1.6	n.d.	2890	0.37	0.81/1.0	NR	NR	Water harvesting at high RH	68
MIL-101-COOH	NR	n.d.	2110	0.39	0.91/1.13	NR	NR	Water harvesting at high RH	68
Co_2Cl_2btdd	NR	2.2	1912	0.28	0.97/1.21	55	30	Water harvesting at medium RH	50
Ni_2Cl_2btdd	NR	2.3	1837	0.32	1.07/1.33	53	400	Water harvesting at medium RH	69
$Ni_2F_{0.83}Cl_{0.17}$btdd	NR	2.3	1770	0.32	1.07/1.33	53	Poor stability	Water harvesting at medium RH	69
Ni_2Br_2btdd	NR	2.2	1530	0.24	0.75/0.93	58	400	Water harvesting at medium RH	69
Cr-soc-MOF-1	2.2	1.7	4549	0.68	1.95/2.43	Room temperature under vacuum	100	Indoor humidity maintenance	70

Table 1 (*continued*)

MOF	Pore volume/nm	Pore size/nm	S_{BET}/m^2 g^{-1}	α	Water adsorption capacity/g g^{-1}/cm^3 g^{-1}	Desorption temperature/°C	Cycling stability	Potential applications	Ref.
BIT-66	0.87	2.58/0.65	1417	0.60	0.71/0.88	Room temperature under vacuum	50	Indoor humidity maintenance	71
UiO-67-4Me-NH_2-38%	0.69	1.6	1638	0.58	0.68/0.85	Room temperature under vacuum	10	Indoor humidity maintenance	21
NU-1500-Cr	1.24	1.4	3580	0.45	1.09/1.36	Room temperature under vacuum	20	Indoor humidity maintenance	72
Zr-adip	0.47	1.28/0.66	1214	0.13	0.43/0.54	70	300	Heat exchanger	73
KMF-1	0.56	0.57	1130	0.14	0.39/0.49	80	50	Heat exchanger	74
AlFFIVE-1-Ni	0.102	n.d.	258	0.02	0.2/0.25	105	15	Dehydration of chemicals	20
kag-MOF-1	0.12	0.38	210	0.05	0.14/0.17	120	NR	Dehydration of chemicals	75
ZJNU-30	1.24	2.1/1.4/0.7	1570	0.25	1.2/1.49	Room temperature under vacuum	NR	Heat exchanger	19

α refers to the relative humidity when it reaches half of the adsorption capacity at 95% relative humidity. Cycle stability refers to the number of cycles that maintain essentially constant performance tested in the reference.

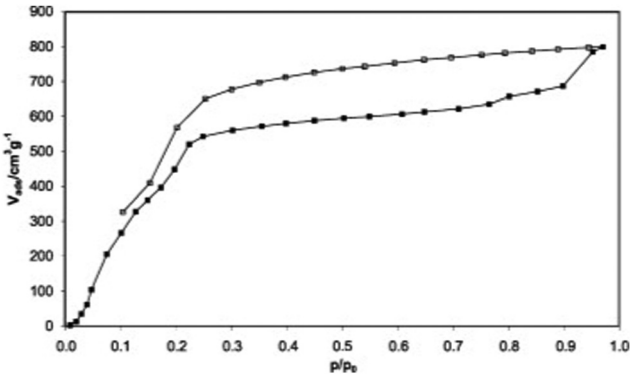

Fig. 4 Water adsorption (solid symbols) and desorption (open symbols) isotherm of HKUST-1 at 25 °C. Reproduced with permission from ref. 37. Copyright 2009, Elsevier Inc. All rights reserved.

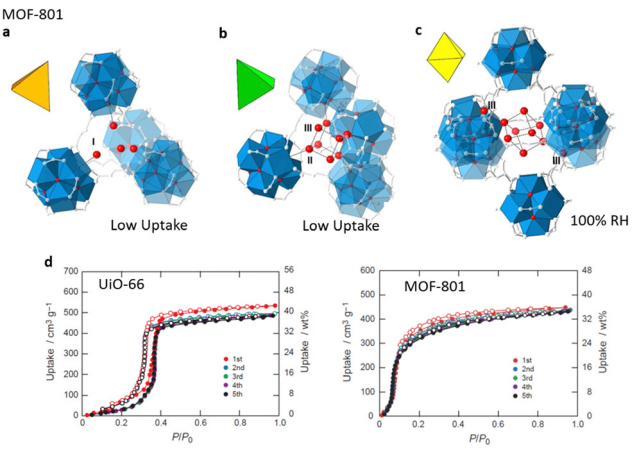

Fig. 5 Water absorption steps in MOF-801 that is composed of tetrahedral cavities (a) and (b) and one octahedral cavity (c). (d) Cycle performance of MOF-801-P and UiO-66 at 25 °C. Reproduced with permission from ref. 39. Copyright 2014, American Chemical Society.

molecules and metal center of Y-shp-MOF-5 prevents around 5 to 6 wt% of water from desorbing at 25 °C. Following the second cycle, the water adsorption isotherm is nearly type V, with a saturation adsorption of 0.45 g g^{-1} which is unaffected after 200 cycles.[7]

ZrMOF-1 ([$Zr_6O_4(OH)_4(H_2O)_8$(pep-1)]), constituted by 8-connected (8-c) cubic $Zr_6O_4(OH)_4(H_2O)_8$ clusters and a rigid 8-c peripherally extended pentiptycene ligand, performed with high stability due to the high coordination numbers. ZrMOF-1 presents two types of cathedral cavities with pore sizes of 11 Å and 19 Å and a large BET surface area of 1877 m^2 g^{-1}. The water absorption isotherm of ZrMOF-1 is proximate to type IV(b). It shows a relatively low water uptake of 0.15 g g^{-1} at a low relative pressure stage (P/P_0 = 0.2) owing to the hydrophobic structure provided by the ligand with a large number of benzene rings. The pore filling takes place at P/P_0 = 0.3 with a water uptake of 0.65 g g^{-1}. ZrMOF-1 has an excellent saturated adsorption capacity of 0.83 g g^{-1} that is only inferior to Ni_2Cl_2btdd, Co_2Cl_2btdd and Ni_2F_2btdd in microporous materials. In addition, ZrMOF-1 has ultra-high stability

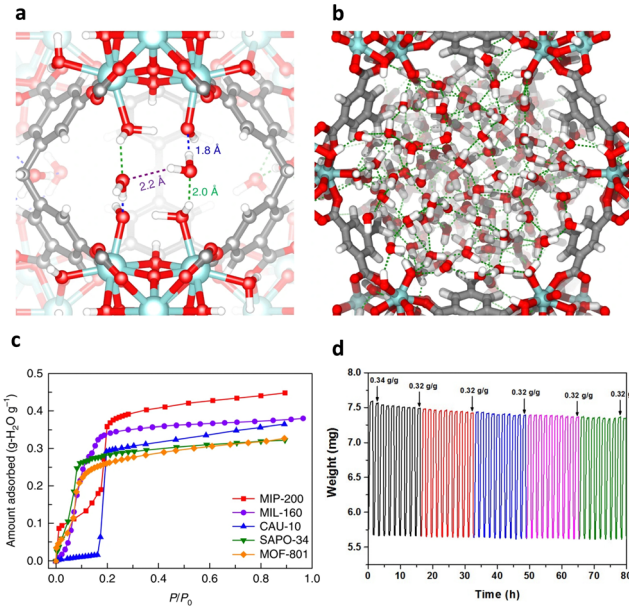

Fig. 6 (a) The initial adsorption sites for water molecules in MIP-200 at low pressure (P/P_0 = 0.01). (b) Densely packed water molecules in the hexagonal channel at saturation (P/P_0 = 0.2). (c) Comparison of the water adsorption isotherms of MIP-200, MIL-160, CAU-10, SAPO-34 and MOF-801 at 30 °C. (d) Thermogravimetric analysis profile for multiple cycles of water adsorption–desorption of MIP-200. Reproduced with permission from ref. 17. Copyright 2018, Springer Nature.

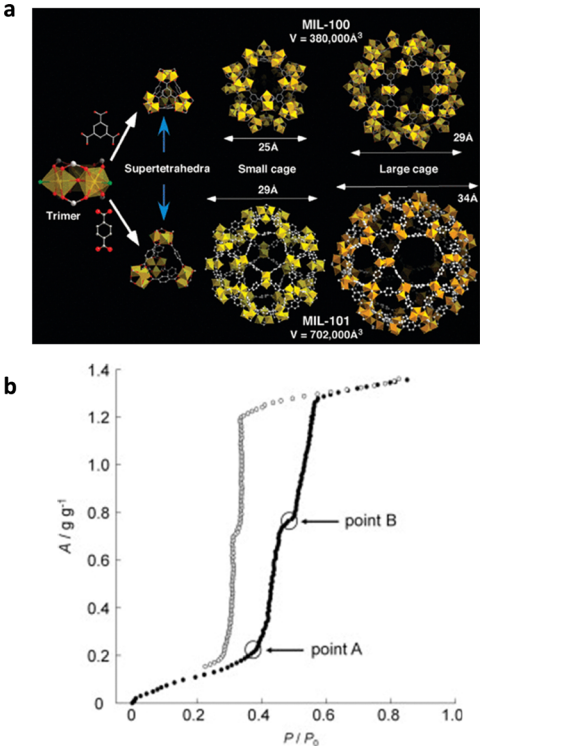

Fig. 7 (a) Structures of the MIL-100 and MIL-101. Reproduced with permission from ref. 85. Copyright 2008, American Chemical Society. (b) Water adsorption (solid symbols) and desorption (open symbols) isotherms of MIL-101 at 25 °C. Reproduced with permission from ref. 86. Copyright 2012, Elsevier Inc. All rights reserved.

that can contain the crystallinity in strong acids/bases and maintains 94% of its original water-absorbing capacity after 500 cycles.[84]

(2) Adsorption properties of mesoporous MOFs. MIL-100 ($[M_3O(H_2O)_2OH(btc)_2]$, M = Fe, Al, Cr), with mesopore sizes of 25 and 29 Å, is one of the most representative mesoporous MOFs for water adsorption (Fig. 7a).[56,85] At low relative pressure ($P/P_0 < 0.25$), the water molecules will first coordinate with metal sites, and then monolayer–multilayer adsorption occurs. When the pressure reaches $0.23 < P/P_0 < 0.4$, irreversible capillary condensation occurs with two water absorption steps sequentially corresponding to the smaller pores and larger pores, leading to the adsorption isotherm similar to the type IV(a). The saturation adsorption uptake of MIL-100(Cr) and MIL-100(Fe) would both be close to 0.8 g g^{-1},[67] whereas MIL-100(Al) has a comparatively low adsorption capacity of approximately 0.50 g g^{-1} due to the lower pore volume caused by the incomplete removal of unreacted ligands. The pore sizes (29 Å and 34 Å) of MIL-101 ($[Cr_3X(H_2O)_2O(bdc)_3]$, X = F, OH) are larger than that of MIL-100.[86] This causes capillary condensation of MIL-101 to occur at a higher relative humidity, specifically, at P/P_0 = 0.4 for small and P/P_0 = 0.45 for large cages respectively (Fig. 7b). Because of the excellent thermal stability, the MIL-100 and MIL-101 series show exceptional cycling stability.[87]

However, capillary condensation does not always occur when the pore diameter is close to the critical diameter (2.076 nm for water at 25 °C).[50] An exceptional example is Co_2Cl_2btdd (H_2btdd = bis(1*H*-1,2,3-triazolo[4,5-*b*],[4′,5′-*i*])dibenzo[1,4]dioxin), also known

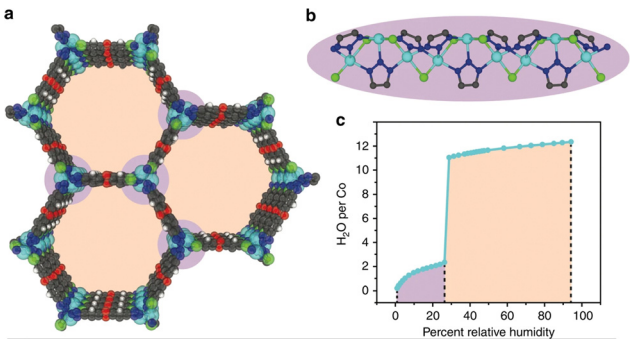

Fig. 8 The honeycomb-like channels (a) and 1D metal chain (b) of Co_2Cl_2btdd viewed along the *z*-axis. (c) Water adsorption isotherm of Co_2Cl_2btdd at 20 °C. Reproduced with permission from ref. 89. Copyright 2019, The Author(s).

as MAF-X27*l*-Cl,[88] with honeycomb one-dimensional pore channels of 2.2 nm which are slightly bigger than 2.076 nm, and the structure of the channel is shown in Fig. 8a and b. At low relative pressure, water molecules first interact with coordination unsaturated Co^{2+} to form water chains by hydrogen bonding, which can reduce the pore width to 2.0 nm, below the critical diameter for capillary condensation.[89] Due to the high hydrophilicity of the $btdd^{2-}$, pore filling of the microporous pores occurred at a relatively low pressure of 0.28, with the adsorption capacity rising

abruptly to 0.97 g g^{-1} (Fig. 8c). The adsorption isotherm approximates type IV(b) with no capillary coalescence. During 30 cycles from 25 °C to 120 °C, the capacity of Co_2Cl_2btdd reduced by 6.3 wt% without losing crystallinity. Co_2Cl_2btdd has a considerably greater water adsorption capacity at P/P_0 = 0.3 (0.87 g g^{-1}) than the mesoporous MIL-101, MIL-100, as well as the microporous CAU-10 and MOF-801.

Ni_2Cl_2btdd is more stable than Co_2Cl_2btdd due to the addition of inert Ni^{2+} to its structure, retaining 98% of its initial mass after 400 cycles. Due to the higher temperature and acid concentration employed in the synthesis of Ni_2Cl_2btdd, a better crystallinity can be obtained. Therefore, Ni_2Cl_2btdd achieved an impressive saturation adsorption capacity of 1.07 g g^{-1}, which is the relatively high water adsorption capacity of all presently available materials with pore filling occurring within 35% RH.[69]

2.3.2 Pore chemistry

(1) Ligands. Generally, the polarity of pore channels can be altered by the polarity of the ligand, affecting the water absorption properties of MOFs. The water adsorption study of the MAF-47 series is one of the pioneering investigations in ligand regulation.[38] Due to the high hydrophobicity of Hmim (2-methylimidazole), MAF-4, also known as ZIF-8, has an extremely low saturation of water absorption of 0.026 g g^{-1} at P/P_0 < 0.9. Fortunately, MAF-7, which was synthesized by replacing the ligand with the more hydrophilic Hmtz (3-methyl-1,2,4-triazole), has a strong water affinity since the uncoordinated N atoms on Hmtz provide extra active sites for guest binding. Although MAF-4 and MAF-7 possess comparable pore volumes and specific surface areas, MAF-7 presents an increased water uptake of 0.443 g g^{-1} and the capillary compensation occurs near P/P_0 = 0.3. MAF-47-*x*, the solid solutions consisting of different molar ratios of Hmim/Hmtz, had a higher pressure of pore filling with increasing proportions of Hmin and similar saturation water uptake with MAF-7, indicating that the H_2O binding affinity can be decreased by reducing the density of active sites on the pore surface (Fig. 9a). Similar strategies were also used in the subsequent MOF-303 studies. MOF-303 [Al(OH)(pzdc)] ($pzdc^{2-}$ = 1-*H*-pyrazole-3,5-dicarboxylate) is isostructural with MOF-333 [Al(OH)(fdc)] (fdc^{2-} = 2,4-furandicarboxylate). Interestingly, H_2pzdc and H_2fdc show different affinities with water molecules, thus the hydrophilicity of the pore can be efficiently regulated by altering the ratio of the two ligands, which enables control of the heats of adsorption (Q_{st}) and desorption temperature. With an increasing degree of fdc^{2-} incorporation, the Q_{st} decreased continuously from 53 to 50 kJ mol^{-1} and the minimal desorption temperature decreased by 10 °C.[41,42]

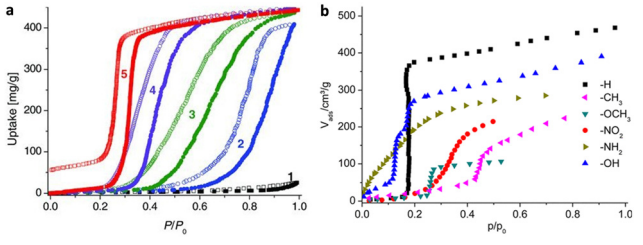

Fig. 9 (a) Water adsorption (solid symbols) and desorption (open symbols) isotherms of MAF-4 (1), MAF-47-0.76 (2), MAF-47-0.49 (3), MAF-47-0.23 (4), and MAF-7 (5) at 25 °C. Reproduced with permission from ref. 38. Copyright 2011, Wiley-VCH Verlag GmbH & Co. KGaA, Weinheim. (b) Water adsorption isotherms of CAU-10-X at 25 °C. Reproduced with permission from ref. 47. Copyright 2013, American Chemical Society.

The water absorption properties of CAU-10 derivatives were extensively explored. For example, CAU-10-X (X = CH_3, OCH_3, NO_2, NH_2 and OH) were synthesized through ligand functionalization to change the polarity, and exhibited a higher water affinity but low saturation adsorption of water due to the smaller effective pore volume.[47] The presence of functional groups alters the polarity, which is principally reflected in the shift of the water adsorption isotherm and even in the change of the adsorption isotherm type. The hydrophilic groups like $-NH_2$ and –OH may boost the polarity and the affinity for water molecules through hydrogen bonding, resulting in a shift of the adsorption isotherm towards the low-pressure region and an increase in capacity at this stage. Given the strong hydrogen bonding between $-NH_2$ and water molecules, the isotherm of CAU-10-NH_2 changes from type II to type I. The introduction of the hydrophobic groups $-CH_3$, $-OCH_3$, and $-NO_2$ increases the hydrophobicity of the pore channel, hence inhibiting the interaction of the CAU-10 derivative with water at low pressure. Consequently, the adsorption isotherm shifts towards higher pressure, eventually increasing the pressure at which pore filling occurs (Fig. 9b). In addition to the modification of functional groups, adjusting the aromatic ring of the ligand may also impact the polarity of the derivative.[90] Numerous different derivatives of CAU-10 were obtained by substituting the benzene ring of the ligand isophthalic acid with the more hydrophilic furan, pyridine, pyrazine, and thiophene, and the more hydrophobic pyrrole, respectively. In particular, the stronger polar hydrophilic aromatic ring increases the affinity for water, resulting in a larger uptake in the low-pressure region and a shift in the pore-filling stage towards lower pressures. The CAU-10 derivative with the highly hydrophilic furan, also known as MIL-160,[91] expresses an approximate type I water adsorption isotherm. The hydrophobic pyrrole, on the other hand, enhances the hydrophobicity of the pore channel, decreasing the adsorption amounts in the low-pressure region and shifting the adsorption isotherm towards higher relative pressures.

Besides the organic ligands, inorganic bridging ligands coupled with metal centres also affect the water adsorption performance of MOFs. By exchanging the coordinated anions, the strength of the hydrogen bond between water and the pore wall can be regulated, which cannot be ascribed only to changes in pore wall polarity.[69] By replacing the μ-Cl^- in Ni_2Cl_2btdd with the more hydrophilic OH^- and F^-, for instance, the resultant $Ni_2(OH)_2$btdd and $Ni_2F_{0.83}Cl_{0.17}$btdd demonstrate an increment in water adsorption at low relative pressure (P/P_0 < 0.1). In contrast to the previously reported phenomenon of hydrophobic pore filling migrating to higher pressure, utilizing the more hydrophobic μ-Br^- as opposed to μ-Cl^- decreases the relative pressure of pore filling from 0.32 to 0.24. Infrared spectroscopy revealed that, due to the high

hydrophilicity of F^- and OH^- groups, $Ni_2(OH)_2$btdd and $Ni_2F_{0.83}Cl_{0.17}$btdd contain a significant proportion of ice-like water with saturated coordination H-bonding bound to the pore wall, providing fewer secondary adsorption sites than liquid-like water with unsaturated coordination H-bonding. With lower hydrophilicity and more liquid water, Ni_2Br_2btdd is more susceptible to pore filling, further implying that, in the presence of strong adsorption sites, the relative pressure for pore filling relies more on the interaction between the water molecules and the water bound to the pore wall than on the polarity of the pore wall itself.

(2) Central metal. Regulating the central metal can also affect the water adsorption behavior.[92] Weak coordination interactions between coordination-unsaturated Zn^{2+} and water molecules in ALP-MOF-1(Zn) ([$Zn_2(\mu\text{-}H_2O)$(alp)(bdc)], H_2alp = allopurinol) contribute to almost negligible water adsorption at low relative pressure ($P/P_0 < 0.23$). In contrast, the coordination between water molecules and Co^{2+} in ALP-MOF-2(Co) [$Co_2(\mu\text{-}H_2O)$-(alp)(bdc)] is much stronger than that with Zn^{2+}, which markedly affects the water absorption behavior at low relative pressure (Fig. 10a). Individual water molecules initially coordinate with unsaturated Co^{2+} and form hydrogen bonds with the skeletal carbonyl oxygen atoms at a relative pressure of 0.04, above which, the adsorption continues with the coordinated water as the secondary adsorption sites until coordination saturation. By altering the Zn/Co metal, a variety of MOFs with distinct water absorption characteristics may be generated, suggesting that the polarity of the central metal can significantly impact the water absorption performance of the MOF, particularly in the low-pressure region (Fig. 10c and d).[66]

2.3.3 Flexibility. Flexible MOF materials possess a breathing effect in adsorption, which is the reversible transition between two states of expansion and contraction when subjected to external stimuli (*e.g.* adsorption and desorption processes),[93,94] presenting a unique water adsorption behavior scarcely observed in other adsorbents.[95] An obvious breathing effect can be

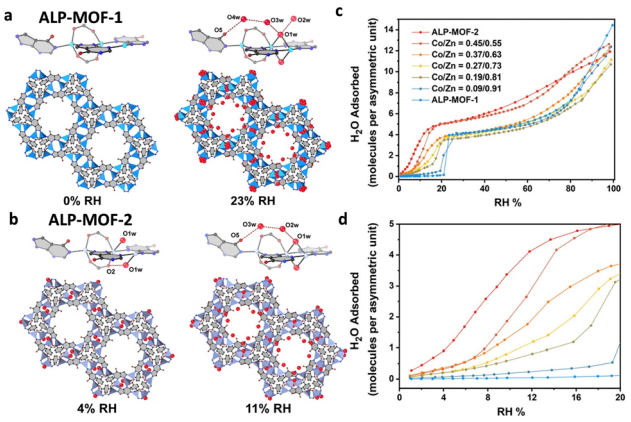

Fig. 10 The stepwise water adsorptions of ALP-MOF-1 (a) and ALP-MOF-2 (b) at low relative humidity. Water adsorption isotherms of ALP-MOFs with different ratios of Co/Zn at (c) 0–100% RH and (d) 0–20% RH. Reproduced with permission from ref. 66. Copyright 2022, American Chemical.

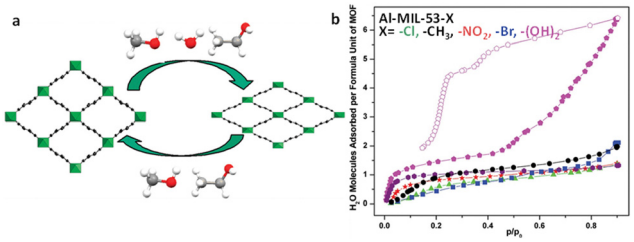

Fig. 11 (a) Structural switching evolution of the MIL-53(Cr) upon adsorption and desorption. Reproduced with permission from ref. 97. Copyright 2010, American Chemical Society. (b) Water adsorption (solid symbols) and desorption (empty symbols) isotherms of the Al-MIL-53-X series at 25 °C. Reproduced with permission from ref. 99. Copyright 2011, American Chemical Society.

observed in the water adsorption process of MIL-53 ([M(OH)-(bdc)], M = Al, Fe, Cr), a typical flexible MOF (Fig. 11a). The fully dehydrated MIL-53(Cr) presents as thermodynamically stable macropores, and when exposed to vapor conditions, the pores shrink to narrow pores, which are stabilized by the interaction of water molecules with the μ_2-OH on the metal cluster and carboxylates on the ligand.[96] MIL-53 series with different metal ions exhibit distinct flexibility, leading to the various behaviors of the breathing effect.[97] Specifically, in the breathing process related with water, MIL-53(Cr) presents a pore shrinkage of 40% compared with the initial size, while 50% for MIL-53(Al) and only 10% for MIL-53 (Fe).[34,98]

Modifications of MIL-53 with functional groups lead to a more complex breathing behavior. In the case of the ligand functionalization of MIL-53(Al), a variety of MIL-53(Al) derivatives containing BDC-X ligands (X = Cl, Br, CH_3, NO_2, $(OH)_2$) were synthesised.[99] In particular, the modified MIL-53 with the BDC-X ligands (X = Cl, Br, CH_3, NO_2) behaved similarly to the unmodified MIL-53(Al), exhibiting a breathing effect with the capture of 1–2 water molecules per unit pore. Meanwhile, the dihydroxy-functionalized MIL-53(Al) collects a single water molecule per unit pore at P/P_0 = 0.1 with subsequent pore shrinkage. Then, it captures an additional five water molecules per unit pore when the relative pressure increases (P/P_0 = 0.4–0.9), which is accompanied by the pore expanding (Fig. 11b). The higher hydrophilicity of the modified backbone may account for this anomaly. Similarly, after the primary adsorption, MIL-53(Al)–$(COOH)_2$ and MIL-53(Fe)–$(COOH)_2$ expressed pore shrinkage, following which the water adsorption continues with further pore expansion.[64,65] Due to the breathing effect, there arises spontaneously a distinct hysteresis loop between adsorption and desorption.

Recently Zaworotko and co-workers reported that a flexible 1D coordination network, [Cu(HQS)(TMBP)] (H_2HQS = 8-hydroxyquinoline-5-sulfonic acid and TMBP = 4,4′-trimethylenedipyridine) can exhibit water vapor-induced reversible structural conformation, showing a stepped sorption profile (type F-IV) at <30% RH.[100] Similarly, X-dia-2-Cd ([$Cd(Imibz)_2$], HImibz = 4-((4-(1*H*-imidazol-1-yl)phenylimino)methyl)benzoic acid) exhibits a similar water-induced transformation. On the other hand, X-dia-2-Cd showed negligible hysteresis due to the very fast transient pore expansion.[101]

3. Application of water-absorbing MOF

3.1 Water harvesting devices

Deserts struggle with water constraint due to little precipitation.[102] Water collection anywhere and anytime satisfies the immediate requirements of people living in extensively arid regions. However, traditional water treatment devices are typically large and intricate, making it difficult to collect water in the arid areas. Fortunately, the atmosphere contains a lot of water vapor, and directly extracting this vapor provides an effective way to solve these challenges.[103] MOFs, with ultrahigh porosity and a tubular pore structure, have been suggested and exploited as absorbents for atmospheric water collection.[104,105]

MOFs used for atmospheric water harvesting should fulfil the following conditions related to the operation environment and energy concerns of water harvesting devices: (1) strong chemical and water cycle stability for the complex conditions in the atmosphere. (2) High water absorption capacity under the operating conditions. (3) Low regeneration temperature. (4) Step-wise water absorption isotherms are favorable because of the large working capacity, but hysteresis loops should be avoided to reduce energy losses.[106]

Typically, the water collecting process consists of three steps: (1) the sorbent absorbs water vapor from the atmosphere at low temperatures and high relative humidity, (2) it releases it by raising the temperature or reducing the relative vapor pressure of the water inside the device, and (3) it then condenses the released water vapor to complete a water collection cycle. During this process, water vapor may be released and condensed naturally or with external energy.

In 2017, Yaghi and co-workers reported the first device for atmospheric water capture and collection using metal–organic frameworks (MOFs), specifically using MOF-801 as the water adsorbent and achieving water collection at a relative humidity of 20%. The device consists of a MOF coating that can be heated and a condensation unit (Fig. 12a and b), and begins water absorption at 25 °C and 20% relative humidity. The waste heat provided by a solar energy between 25 °C and 65 °C is used as the driving force for circulation (Fig. 12c and d). MOF-801 exhibits a steep adsorption isotherm at P/P_0 = 0.08, with an adsorption capacity of up to 0.29 g g^{-1} at 25 °C and a relative humidity of 20% (Fig. 12e and f); therefore, the device is estimated to theoretically capture 0.24 L of water per kilogram of MOF per day. Due to the hydrophilicity of MOF-801, the regeneration temperature is as low as 65 °C, allowing for easy regeneration conditions such as using the low heat of natural sunlight, which negates the need for additional energy input.[15]

Passive water collection devices employ solar energy for absorption and desorption processes without additional energy input, using air as the heat sink. The passive device operates only one cycle each day, with poor time efficiency, and water productivity mostly relies on the maximal adsorption capacity of MOFs. Due to the limitations of thermal conductivity and solar absorption capacity, a large number of adsorbents must be employed to satisfy the daily demands of an individual (3.5 liters),[107] necessitating relatively expensive apparatus.

To increase apparatus productivity and decrease associated costs, it is preferable to design active water collection systems that can be repeatedly cycled and require minimal energy input. The active collection device absorbs and releases water with the aid of external energy sources, such as electricity for heating, refrigeration, and condensation. The optimal adsorbent for the active water collection system requires rapid water uptake and release kinetics and a low regeneration temperature. Among the various adsorbent options, MOF-303 stands out as the most promising candidate for the water collection system. At a temperature of 30 °C, MOF-303 exhibits a sharp

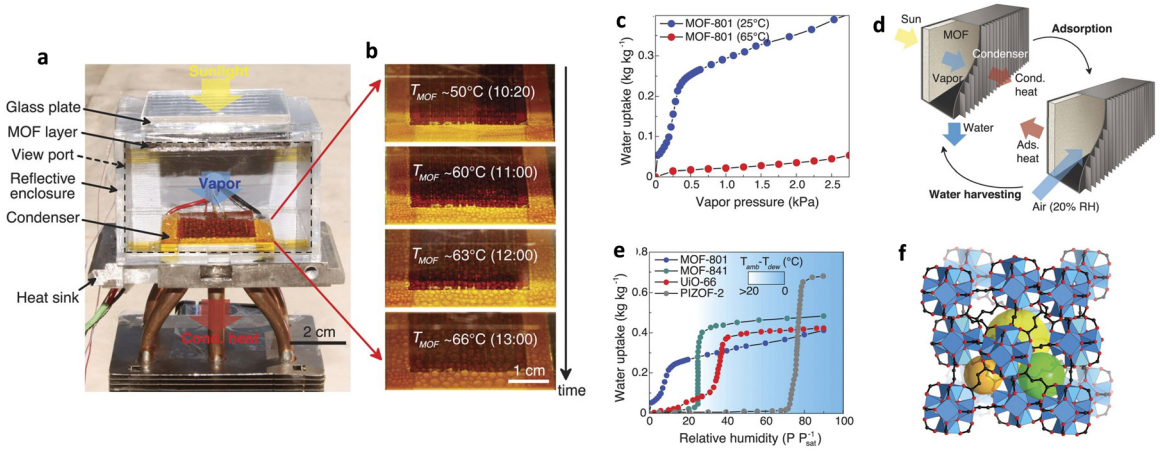

Fig. 12 (a) Image of a water harvesting device with MOF-801 as the water adsorbent. (b) Formation and growth of water droplets as a function of MOF temperatures (T_{MOF}) and local time of day. (c) Water-adsorption isotherms of MOF-801 at 25 °C and 65 °C, respectively. (d) A MOF water-harvesting system, composed of a MOF layer and a condenser, undergoing solar-assisted water-harvesting and adsorption processes. (e) Water adsorption isotherms of MOF-801, MOF-841, UiO-66, and PIZOF-2 at 25 °C. The background color map shows the minimum difference between the temperatures of the ambient air (T_{amb}) and the condenser (T_{dew}) required for dew collection with active cooling. (f) Crystal structure of MOF-801. Reproduced with permission from ref. 15. Copyright 2017, American Association for the Advancement of Science.

adsorption uptake at a relative pressure of P/P_0 = 0.12, with a maximum adsorption capacity of 0.40 g g^{-1} at a relative humidity of 30%. MOF-303 has a low adsorption enthalpy of approximately 52 kJ mol^{-1} and shows fast adsorption rates at both 30% and 40% relative humidity, outperforming SAPO-34, Zeolite 13X, and aluminum fumarate in this aspect. Furthermore, MOF-303 displays rapid desorption rates, with complete desorption achieved within one hour at 85 °C and even faster at higher temperatures, which is significantly shorter than the desorption times for SAPO-34 and Zeolite 13X. Notably, a 3 mm bed of MOF-303 can be fully dehydrated within a few minutes of mild heating (85–100 °C). An active water harvesting device was fabricated using MOF-303, which was subjected to adsorption at 27 °C and 32% relative humidity, followed by desorption at 85 °C. The device was cycled nine times over a 24 hour period, yielding a water production rate of 1.3 L kg_{MOF}^{-1}, which is significantly higher than that of passive water harvesting devices. In comparison, a device using aluminum fumarate as the adsorbent only produced 0.55 L kg_{MOF}^{-1} under the same conditions, highlighting the superior dynamic water uptake performance of MOF-303 over other adsorbents.[108]

Besides passive and active water harvesting, a self-adaptive water harvesting system that optimizes the duration and efficacy of each cycle based on external environmental conditions has been developed. The system employs an algorithm to ensure the shortest possible cycle time is accomplished regardless of the environmental conditions. The adaptive water harvesting system combines the relative humidity and temperature of the external environment with the dew point value to configure the water collection device (Fig. 13a). The measured dew point is obtained in real-time, and the steady-state dew point value is chosen as the endpoint for adsorption, while the maximal dew point value is chosen as the endpoint for desorption. As a guide for adsorption and desorption, the external temperature corresponding to the maximal dew point value is used as the heating temperature. The system has the potential to considerably increase the efficacy and effectiveness of water harvesting devices, especially in arid regions with limited water resources. Compared to an active water harvesting device, a self-adaptive device with MOF-801 as the sorbent was shown to produce up to 26% more water (2.6 L_{H_2O} $kg_{MOF\text{-}801}^{-1}$ d^{-1}) (3.52 L_{H_2O} $kg_{MOF\text{-}801}^{-1}$ d^{-1}). In addition, the self-adaptive device reduces to 1.5 cycles per day, reducing energy consumption by 20–44% under the same climatic conditions. Furthermore, the self-adaptive device was verified to produce water continuously and consistently with no performance degradation after operating for over a year (Fig. 13b and e).[109]

Ni_2Cl_2btdd achieves an ultra-high water uptake of 0.9 g g^{-1} at 40% RH and shows great potential for atmospheric water absorption. Wang and Zhang *et al.* achieved striking progress in the passive water absorption device area.[110] By using Ni_2Cl_2btdd and materializing the precise temperature zoning inside the suction unit, highly efficient water desorption and condensation was achieved with a small device. In the device, the heating temperature can barely reach 97 °C through direct solar radiation with the effect of double insulation layers and a

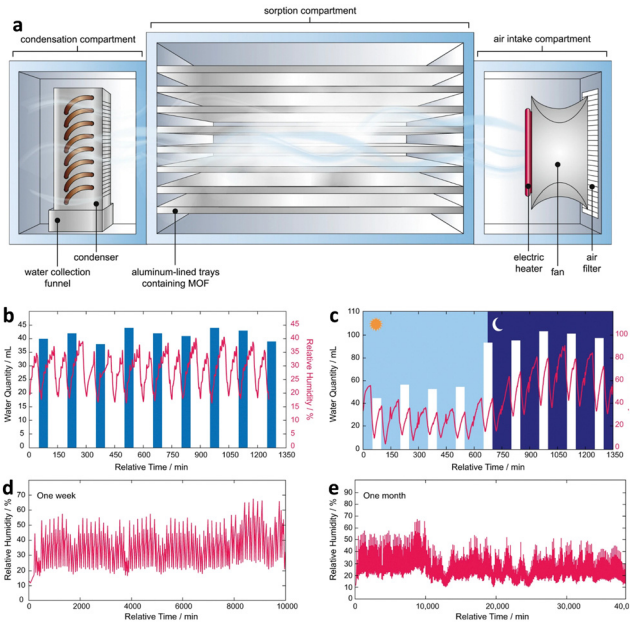

Fig. 13 (a) Schematic of the atmospheric water harvester. (b) Stress test for 24 h performed under a controlled environment (20% RH and 25 °C). (c) Assessment of real-world performance over a full day. (d) Real-environment continuous performance for one week. (e) Performance of self-adaptive water harvesting devices during continuous operation for a month. Reproduced with permission from ref. 109. Copyright 2022, The Author(s).

photothermal plate. At the same time, the cooling part can achieve efficient condensation in the temperature difference of 60 °C due to the existence of vibrating fins. The device could obtain 0.495 L_{H_2O} kg_{MOF}^{-1} after running one cycle (7 h) at 30 °C 40% RH and with 1000 W of light. Furthermore, the average unit volume and unit area water yield are 19.63 L m^{-3} and 717.25 g m^{-2} respectively, which are comparable to the previous device's use of 6.67 kg m^{-2} MOF and in the case of using only 1.45 kg m^{-2} MOF in the new device.

MOFs with water absorption stages greater than 30% RH can be utilized in arid water collection systems if a cooling source is incorporated into the adsorption device. When the temperature within the device is lowered, the relative humidity increases due to the reduction in saturated vapor pressure, which can exceed 30% RH compared to the external environment. Under these conditions, MOFs with water uptake steps at moderate relative humidity can be utilized for water harvesting. MIL-101 exhibits water absorption steps greater than 35% RH, with an adsorption capacity of 0.106 g g^{-1} at 30% RH and 25 °C in the external environment. When the cooling device is activated and the temperature within the device reaches 14 °C, the adsorption capacity of MIL-101 increases considerably to 1.05 g g^{-1} at a rapid rate. The majority of water can be desorbed from MIL-101 without additional heating after the cooling device has been deactivated. The average functional capacity per cycle is 0.77 g g^{-1} under conditions of 23 °C and 30% RH. Under optimal conditions, if the cooling device is activated for 20 minutes every 20 minutes, the predicted water collection rate can reach 27 L kg^{-1} day^{-1},

which is significantly higher than current water harvesting devices made from MOF-303 and MOF-801.[111] However, the high energy usage and maintenance requirements of the condenser apparatus are disadvantages of the improved condensation efficacy.

The development of MOFs for water collection has led to improvements in devices as well as the widespread development of MOF-based composite materials that can increase water absorption capacity and ease of regeneration through the synergistic effect of MOFs and other components, allowing them to adapt to various adsorption environments. Due to the outstanding photothermal property and thermal conductivity of carbon-based materials, the ability of MOFs complexed with carbon-based materials to speed up adsorption and analysis has been investigated. Du and co-workers have synthesized high water-absorbing photothermal composite materials composed of MOF-801 and carbon nanotubes (CNTs), which exhibit a good water absorption capacity and fast adsorption and desorption rates. This has contributed to the investigation of adding carbon materials to enhance the photothermal performance of water adsorbents.[112]

MOF-hydrogel composites have been applied to tropical regions with high relative humidity, in addition to water collection devices designed for arid regions. Using MIL-101(Cr) as a water-absorbing agent, which has a large adsorption capacity for water at high humidity (P/P_0 = 0.9), and the hydrophilic polymer PNIPAM [poly(*n*-isopropylacrylate)] as a continuous water-absorbing matrix, a porous PC-MOF (polymer composite-MOF) water absorb-supply material with a strong outer wall was prepared (Fig. 14a). MIL-101 exhibited a precipitous water absorption trend between relative pressures of 0.4 and 0.5, and the saturation water uptake at 25 °C was as high as 1.4 g g^{-1}. By combining the exceptional water absorption performance of MIL-101 with the continuous water absorption of PNIPAM, a sustainable process for atmosphere-water harvesting can be attained. MIL-101 captures water molecules from the environment, and since PNIPAM cannot expand to water absorption saturation due to the strength of the composite outer wall, it constantly absorbs and releases the water in MOFs (Fig. 14b). The system generates 6 grams of fresh water per gram sorbent per day with a total water delivery efficiency of 95% and an automated water delivery efficiency of 71% at 90% RH, the highest stated record for atmospheric water harvesting devices without heat sources.[113] The related water absorption properties of the above devices are summarized in Table 2.

3.2 Indoor humidity maintenance

In contemporary times, individuals tend to spend a significant portion of their diurnal activities and routines within enclosed indoor spaces. As recommended by the American Society of Heating, refrigerating and air-conditioning engineers (ASHRAE), maintaining indoor relative humidity levels between 45% and 65% is deemed optimal for ensuring human well-being

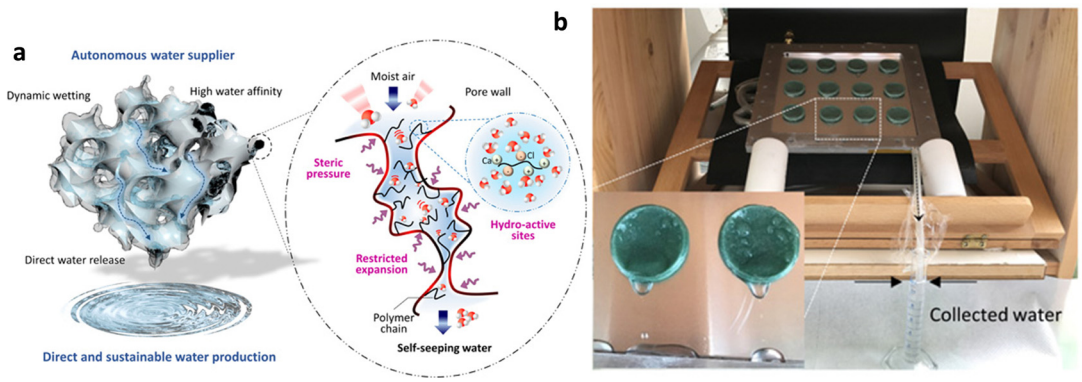

Fig. 14 (a) Schematic illustration of polymer–MOF hybrid materials for self-seeping water. (b) Image of the proof-of-concept prototype for atmospheric water harvesting. Reproduced with permission from ref. 113. Copyright 2020, The Authors.

Table 2 Summary of the performance in water absorption MOF devices

Types of MOF	Device type	Humidity and temperature for water absorption	Humidity and temperature for water desorption	Daily water output	Cycle times of one day	Ref.
MOF-801	Passive water harvesting	25 °C, 20% RH	65 °C, 20% RH	0.24 L kg^{-1} day^{-1}	1	15
MOF-303	Positive water harvesting	27 °C, 32% RH	80–120 °C, 32% RH	1.3 L kg^{-1} day^{-1}	9	108
MOF-801	Self-adaptive water harvesting	15–35 °C, 17–32% RH	Environment temperature corresponding to the dew point	3.52 L kg^{-1} day^{-1}	Depends on the environmental Conditions from 6 to >30 cycles daily	109
MIL-101	Water harvesting by inner cooling device	Outside 25 °C, 30% RH, inside 14 °C	30% RH, 25 °C	27 L kg^{-1} day^{-1}	35	111
MIL-101	Autonomous water collection	25 °C, 90% RH	No desorption required	6 L kg^{-1} day^{-1}	Autonomous self-supplement water harvesting	113

and comfort.[114] Deviations from this range, either in excess or deficiency, can adversely affect human health.[115]

To regulate indoor RH levels, it is possible to utilize suitable water adsorption materials that can rapidly adsorb water vapor when the humidity level exceeds 65% RH and desorb it quickly when the RH level falls below 45% RH. Considering practical applications, the ideal MOF for indoor humidity control should exhibit a robust water absorption performance and high adsorption capacity, featuring an S-shaped adsorption curve with a steep absorption trend between 45% and 65% and an obvious hysteresis loop concentrated in 45–65%.

Y-shp-MOF-5 is the first MOF applied for indoor humidity control, which exhibits an S-shaped water adsorption isotherm at room temperature, with an adsorption capacity of 0.33 g g^{-1} at a RH of 65% and a saturated adsorption capacity of 0.50 g g^{-1}. In a hermetically sealed environment with variable RH levels, when the RH level was slightly above 65%, Y-shp-MOF-5 adsorbed water vapor until the RH level dropped below 45% or the material reached its saturated adsorption capacity of 0.50 g g^{-1}. Subsequently, when the humidity level fell below 45%, Y-shp-MOF-5 underwent desorption, releasing water molecules into the atmosphere and restoring the humidity to a level between 45% and 65%. Furthermore, Y-shp-MOF-5 exhibited excellent cycling performance, with no change in working capacity after 1000 cycles of adsorption at 85% RH and desorption at 25% RH. However, in the case where the relative humidity is drastically higher than 65% RH (*e.g.*, 70–80% RH) and drastically lower than 45% RH (*e.g.*, 35–25% RH), automatic dehumidification/humidification is required because the working capacity of the material is limited, and the sample is saturated by adsorption or desorbed completely.[7]

Cr-soc-MOF-1 ($[Fe_3(\mu_3\text{-}O)(H_2O)_2(tcpt)_{1.5}Cl]$ H_4tcpt = 3,3″,5,5″-tetrakis(4-carboxyphenyl)-*p*-terphenyl) exhibits an S-shaped water adsorption isotherm, with a steep adsorption trend between 60% and 70% RH and desorption occurs between 35% and 45% RH, satisfying the requirements of ASHRAE for indoor humidity control. Therefore, Cr-soc-MOF-1 can also be applied for indoor humidity control. Compared to Y-shp-MOF-5, Cr-soc-MOF-1 has a significantly higher surface area (BET specific surface area of 4549 m^2 g^{-1}) and water adsorption capacity (1.95 g g^{-1} at room temperature), which is approximately four times that of Y-shp-MOF-5. Additionally, Cr-soc-MOF-1 also exhibits excellent cycling stability, with no change in water adsorption performance observed after 100 adsorption–desorption cycles conducted between 25% and 85% RH.[70]

BIT-66 ($[V_3(O)_3(H_2O)(btb)_2]$ H_3btb = 1,3,5-tris(4-carboxyphenyl)benzene) demonstrates an S-shaped water adsorption isotherm, with adsorption primarily occurring between 55% and 65% RH and desorption occurring between 45–50% RH, accompanied by a noticeable hysteresis phenomenon. According to the working humidity range required by ASHRAE, BIT-66 shows a fairly high working capacity of approximately 0.45 g g^{-1}, while the water capacity of Y-shp-MOF-5 was about 0.017 g g^{-1} within this working range. Although NU-1500-Cr exhibits a higher working capacity of approximately 0.86 g g^{-1}, it has no significant hysteresis. Therefore, BIT-66 with a large hysteresis loop is better suited for maintaining indoor humidity. The indoor environment is also confronted by the intricate issue of mould, fungi and bacteria, especially under high humidity conditions. Fortunately, BIT-66 possesses both moisture tunability ability and bacteriostatic activity, which can effectively eliminate *E. coli* by producing reactive oxygen species under visible light irradiation.[71]

CAU-1-OH, built by functioning CAU-1, can be used as a humidity control agent with the bacteriostatic effect. The adsorption step of CAU-1-OH is mainly in the range of 40–60% RH, and the desorption process is mainly concentrated in the range of 30–50% RH, with a saturation adsorption capacity of *ca.* 0.45 g g^{-1}. The working capacity of CAU-1-OH is significantly higher than Y-SHP-MOF-5 and Cr-soc-MOF-1. Importantly, CAU-1-OH is more applicable to daily life because of the high natural abundance and low toxicity of aluminum. Moreover, CAU-1-OH has a strong photocatalytic anti-bacterial ability, and the inactivation rate of *E. coli* reaches 99.94% after 2 hours of visible light irradiation.[8]

UiO-67-4Me-NH_2-38% with a good adsorption ability was synthesized by ligand exchange on the basis of UiO-67. The introduction of methyl groups increased its hydrophobicity, resulting in an S-shaped adsorption isotherm with steep adsorption occurring between 55% and 65% and desorption concentrated between 45% and 55%. The inflection points of adsorption and desorption are entirely within the ASHRAE range, with a maximum adsorption capacity of approximately 0.65 g g^{-1}. When the adsorption humidity is selected as 65% and 40% for the desorption humidity, the working capacity is approximately 0.52 g g^{-1}, higher than that of BIT-66, Y-shp-MOF-5, and Cr-soc-MOF-1. And the related water absorption properties of indoor humidity maintenance are summarised in Table 3. In a 60 m^3 room at 25 °C, increasing the humidity from 0 to 65% RH required 1.495 kg of UiO-67-4Me-NH_2-38%, while decreasing the humidity from 100% to 65% RH required 0.805 kg of UiO-67-4Me-NH_2-38%. In addition, UiO-67-4Me-NH_2-

Table 3 Summary of properties for indoor humidity maintenance MOF

Material	Tigger point (RH)	Water uptake (wt%)		Working capacity (wt%)	Ref.
		40% RH des	65% RH ads		
Y-shp-MOF-5	55%	27	28.7	1.7	7
Cr-soc-MOF-1	60%	73.5	56	NA	70
NU-1500-Cr	44%	16.6	102.4	85.8	72
BIT-66	56%	9.44	54.83	45.39	71
UiO-67-4Me-NH_2-38%	55%	8	60	52	21

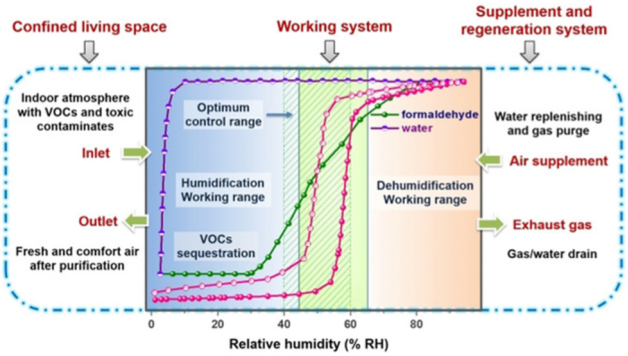

Fig. 15 Indoor humidity maintenance isotherms and breakthrough curves with formaldehyde/water vapors of UiO-67-4Me-NH_2-38%. Reproduced with permission from ref. 21. Copyright 2021, Wiley-VCH GmbH.

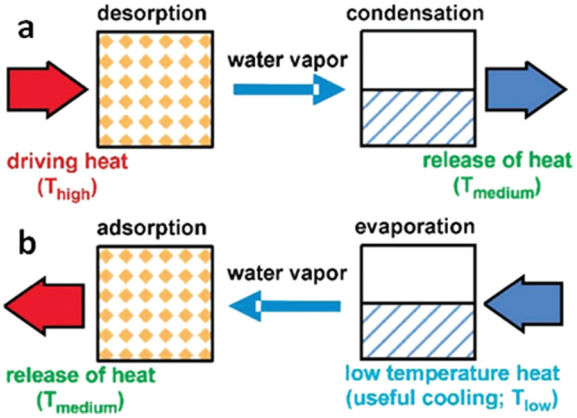

Fig. 16 Principle process in a water adsorption heat exchanger: (a) In the regeneration or desorption process, the water in the pore channel is desorbed by external heat, and the released water vapor condenses in the condenser, which releases the condensed heat into the environment. (b) In the adsorption process, the adsorbent releases heat by absorbing water vapor, thus causing an increase in temperature, while the container containing water absorbs heat due to the evaporation of water, resulting in a decrease in ambient temperature. Reproduced with permission from ref. 119. Copyright 2009, American Chemical Society.

38% preferentially captures formaldehyde, NH_3, benzene, toluene, and *n*-hexane in the presence of both water and gaseous pollutants, achieving both humidity control and indoor air purification (Fig. 15).[21]

3.3 Water adsorption heat exchanger

Due to frequent harsh weather, heating and cooling equipment demand has been rising. Conventional refrigerators and air conditioners utilize extremely combustible and poisonous chlorofluorocarbon refrigerants, which are environmentally hazardous and only 3–10% efficient. Therefore, developing eco-friendly and effective cooling and heating technology is crucial.[116] Heat-driven adsorption heat exchangers, which use low-temperature waste heat or solar energy as the major energy source, may help solve energy and environmental issues.[117] Water is an ecologically favorable adsorbate due to its high enthalpy of evaporation (40.7 kJ mol^{-1}) and non-polluting nature.[118,119]

Water adsorption heat exchanger operation is depicted in Fig. 16. In the process of regeneration or desorption of the adsorbent, the water in the pore channel is desorbed using external heat, and the liberated water vapor condenses in the condenser, releasing heat into the environment, as illustrated in Fig. 16a. In the adsorption process, adsorbents release heat by absorbing water vapor, which raises the temperature. The water container absorbs heat and lowers the ambient temperature owing to evaporation (Fig. 16b). The working conditions of the adsorption heat exchanger are determined by three temperatures, (1) high temperature (T_{high}) for regeneration and desorption, (2) medium temperature (T_{medium}) for condensation and adsorption of water by the adsorbent, and (3) low temperature (T_{low}) for water evaporation. The energy utilization efficiency can be characterized by a coefficient of performance (COP) under the same working conditions. Typically, for refrigeration systems, the COP_C is defined as the energy absorbed from the environment by the evaporation of the working fluid in the evaporation chamber (Q_{ev}) divided by the energy required to regenerate the adsorbent (Q_{regen}), a value that is normally less than 1.[119]

$$COP_C = \frac{Q_{ev}}{Q_{regen}}$$

Various MOFs exhibiting excellent water absorption performance with steep adsorption isotherms and low regeneration temperatures, are considered promising candidates as solid adsorbents for water adsorption heat exchangers.[119,120] ISE-1 ($[Ni_3(\mu_3\text{-btc})_2(\mu_4\text{-btre})_2(\mu\text{-}H_2O)_2]$, btre = 1,2-bis(1,2,4-triazol-4-yl)ethane) was the first MOF to be used as an adsorption heat exchange material, before that silica gel was commonly used as a heat exchange material. At the operating conditions of 95 °C (T_{high})/40 °C (T_{medium}) in the adsorption chamber and 10 °C (T_{low}) in the evaporation chamber, the working capacity of ISE-1 was 50 g kg^{-1} and that of silica gel was 40 g kg^{-1}, both considerably higher than that of adsorbents such as zeolite. Subsequently, a growing number of MOFs showed potential for heat exchange applications.[121]

Due to its availability and simplicity of manufacture, stable microporous aluminium fumarate is a good candidate for water adsorption heat exchangers. Microporous aluminum fumarate exhibits a characteristic steep S-shaped isotherm with a maximum adsorption capacity of 0.35 g g^{-1} at $0.20 < P/P_0 < 0.35$ and outstanding cycle stability.[122] The thermal gradient technique allows it to develop directly on the metal substrate, and the excellent thermal coupling between the MOF and aluminium plate promotes heat transmission and remains stable after 4500 adsorption/desorption cycles.[55] Afterward, microporous aluminium fumarate heat exchangers were investigated and fabricated. Microporous aluminium fumarate was directly synthesized with polysiloxane binders coated on aluminium plates to make water adsorption full-size heat exchangers. Under the operating conditions of the actual adsorption refrigerator, with the adsorption chamber at 90 °C (T_{high})/30 °C (T_{medium}) and the evaporation chamber at 18 °C (T_{low}), the maximum cooling power of the devices was 2900 W with an average of 690 W, and the maximum specific volume cooling power was 430 W L^{-1}, with an average of 101 W L^{-1}.

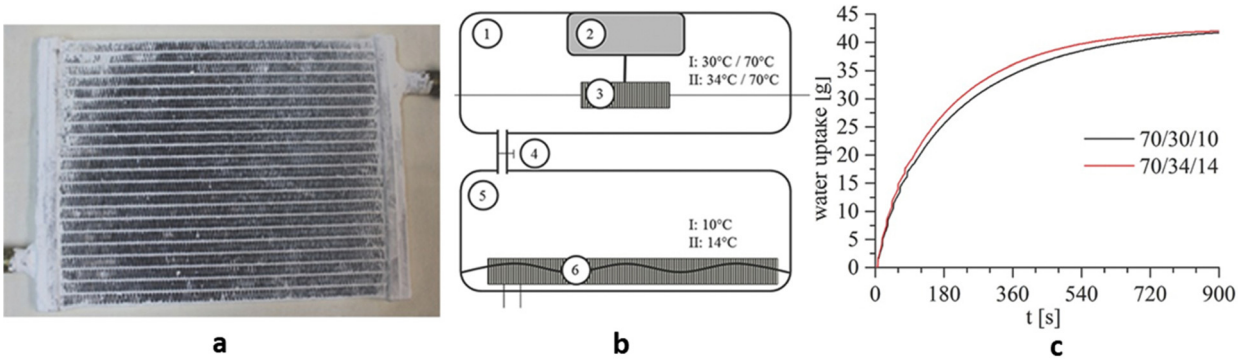

Fig. 17 (a) Image of a coated heating exchanger. (b) Schematic setup of the measurement device with 1 adsorption chamber, 2 balance, 3 adsorber with hydraulic connections, 4 valve, 5 evaporator chamber, and 6 evaporator in water with hydraulic connections. (c) Overall water uptake of the coated heating exchangers. Reproduced with permission from ref. 18. Copyright 2017, Wiley-VCH Verlag GmbH & Co. KGaA, Weinheim.

The material may regenerate below 65 °C, enabling the system to be more efficient and energy-saving. At an evaporation chamber temperature of 22 °C, the device cooling efficiency (COP_C) reaches 0.72 at a heat source of 65 °C and a heat dissipation temperature of 35 °C.[123]

Because of the high water uptake, low cost, and good water stability, CAU-10-H was used to make adsorption heat exchangers by Stock and co-workers (Fig. 17a). At 70 °C driving heat temperatures, the CAU-10-H coated heat exchanger had an excellent working capacity (0.256 g g^{-1}) but only increased 0.018 g g^{-1} by raising the temperature to 150 °C. The adsorption heat exchanger works reliably at 70 °C (T_{high})/34 °C (T_{medium}) in the adsorption chamber and 10 °C (T_{low}) in the evaporation chamber (Fig. 17b), with a volumetric specific cooling power of 229 W L^{-1} and a specific cooling power of 1369 W kg_{Ads}^{-1}. Its rapid adsorption kinetics of 0.6 g kg_{Ads}^{-1} s^{-1} took 430 s from 0 to 90% loading (Fig. 17c). The power output averaged 215 W, more than most silica-aluminate heat exchangers. The power of existing silica-aluminate water adsorption heat exchangers is in the range of 79–230 W. Furthermore, CAU-10-H only needs to be regenerative at 70 °C, which is lower than the driving temperature of water adsorbents such as silica-alumina phosphate and zeolite, enabling effective use of low-temperature heat sources such as waste heat and solar thermal collectors.[18]

MOF-841 ($[Zr_6O_4(OH)_4(mtb)_2(HCOO)_4(H_2O)_4]$, H_4mtb = tetrahedral methanetetrabenzoic acid) exhibited high reversibility of water absorption with an S-shaped adsorption curve. Due to the lower Q_{st} (50.4 kJ mol^{-1}) of MOF-841 in contrast to the MOF-801 series, the COP_C of MOF-841 can reach 0.83 at operating conditions of 70 °C (T_{high})/45 °C (T_{medium}) for the adsorption chamber and 15 °C (T_{low}) for the evaporation chamber.[124]

KMF-2 is synthesized by replacing half of the ipa^{2-} ligand in CAU-10 with 3,5-pyridinedicarboxylate ($pydc^{2-}$). Due to the more hydrophilic structure of KMF-2, the water absorption step moves to the lower pressure region and the water absorption capacity attains 0.32 g g^{-1} at P/P_0 = 0.2. At 70 °C/30 °C in the adsorption chamber and 5 °C in the evaporation chamber, and KMF-2 performed a higher COP_C of 0.75 exceeding CAU-10 (0.72).[125]

During experiments conducted under adsorption conditions of 30 °C/RH 35% and desorption conditions of 63 °C/RH 10%, MIP-200 demonstrated a steep adsorption curve at a P/P_0 of 0.25 and a working capacity of 0.3 g g^{-1}, higher than that of CAU-10-H (0.27 g g^{-1}), MIL-160 (0.24 g g^{-1}) and MOF-801 (0.14 g g^{-1}). The COP_C of MIP-200 increased with increasing desorption temperature within the range of 55–70 °C at an evaporation chamber temperature of 5 °C and a mid-temperature of 30 °C during adsorption. Furthermore, the COP_C of MIP-200 was higher than that of commonly used solid adsorbents such as MIL-160, CAU-10, and MOF-801 at desorption temperatures of 60–100 °C.[17]

By replacing the bridging $-CH_2$ on the MIP-200 ligand with –NH, the resulting MOF (Zr-adip) bearing Lewis base N sites shows increased hydrophilicity. Zr-adip achieved a high water uptake of 0.43 g g^{-1} at 30 °C and P/P_0 = 0.25, which is higher than MIP-200 (0.39 g g^{-1}), KMF-1 (0.39 g g^{-1}) and MOF-303 (0.38 g g^{-1}). And at 70 °C/30 °C in the adsorption chamber and 5 °C in the evaporation chamber, the COPc of Zr-adip (0.79) was slightly higher than MIP-200 (0.78), KMF-1 (0.75) and MOF-303 (0.72), showing a favourable energy utilization efficiency for the heat exchanger.[73] Similarly, UiO-66-N, built by replacing the benzene ring of the UiO-66 ligand with pyridine, generated a higher water capacity (0.37 g g^{-1}) and the adsorption step moved to lower pressure as the introduced N atom strengthens the hydrophilicity. At the adsorption temperature of 30 °C, evaporation temperature of 5 °C, and desorption temperature of 65 °C, the COP_C of UiO-66-N was 0.71, much higher than that of UiO-66 (0.50), and better than well-performing CAU-23 (0.34), KMF-1 (0.42), MIL-160 (0.51), and MOF-303 (0.61).[60] ZJNU-30 possessed steep adsorption at P/P_0 of 0.22 and reached saturation rapidly without stepwise adsorption, achieving an exceedingly high working capacity of 1.2 g g^{-1}, larger than that of MOF-841. Since ZJNU-30 ($[Zr_9O_6(OH)_6(PhCOO)_6(L)_4]$, L = 4,4′,4″-benzene-1,3,5-triyl-1,1′,1″-trinaphthoic acid) consists of three interconnected cages of different sizes (7 Å, 14 Å and 21 Å),[126] the initial adsorption of water molecules occurs in the small cages at low relative pressures, which subsequently diffuses into the other connected cages, avoiding the capillary condensation that commonly occurs in mesoporous materials and ensuring low initial adsorption pressures. As ZJNU-30 showed no irreversible capillary condensation, it featured a particularly

low desorption temperature of about 30 °C. At the operating conditions of 30 °C/25 °C in the adsorption chamber and 10 °C in the evaporation chamber, it provided the highest COP_C reported to date, up to 0.948, showing great potential for application in the field of water adsorption heat exchange.[19]

3.4 Dehydration of chemicals

Natural gas is normally transported by pipeline systems, but the presence of water can cause corrosion of metal pipelines.[127,128] Eddaoudi and co-workers reported the water adsorption MOFs of AlFFIVE-1-Ni (KAUST-8, $[NiAlF_5(H_2O)(pyr)_2]\cdot 2(H_2O)$, pyr = pyrazine) and FeFFIVE-1-Ni (KAUST-9, $[NiFeF_5(H_2O)(pyr)_2]\cdot 4(H_2O)$) used for nature gas dehydration (Fig. 18a). The water uptakes of AlFFIVE-1-Ni and FeFFIVE-1-Ni increased sharply at relative humidity close to 0 due to the presence of OMS (Fig. 18b). At P/P_0 = 0.05 the adsorption amounts of the two were 0.22 g g^{-1} and 0.18 g g^{-1}, respectively, which were higher than most commercially used solid adsorbents such as 3A and 13X. Besides, the heats of adsorption for the two were 63 kJ mol^{-1} and 65 kJ mol^{-1}, respectively, which were far lower than that of zeolites 3A, 4A and 5A (80–120 kJ mol^{-1}), and thus possessed a lower regeneration temperature of *ca.* 105 °C (Fig. 18c). In addition, both AlFFIVE-1-Ni and FeFFIVE-1-Ni demonstrated excellent cycling stability, with no discernible change in performance after 15 cycles (Fig. 18d). Thus, it is evident that AlFFIVE-1-Ni and FeFFIVE-1-Ni satisfy the requirements for natural gas dehydration adsorbents, which was further demonstrated by the breakthrough experiment with a mixture of CO_2/CH_4 (v/v = 1/99) at RH of 75%. Changing the gas to CO_2/N_2 and increasing the CO_2 concentration to 1, 10, and 50% did not significantly affect the water vapor retention time, indicating excellent dehydration performance (Fig. 18e–h).[20]

Kag-MOF-1 $[Zn(HCN_4)_2,(H_2O)_{2/9}]$ possessed honeycomb one-dimensional pore channels with a pore size of approximately 3.8, while retaining fine crystallinity at pH = 4 and pH = 10. Fully activated kag-MOF-1 possesses metal sites that are accessible for coordination with water molecules. In the meantime, the N atoms in the ligand increase the hydrophilicity of the channel, resulting in the formation of hydrogen bonds with water molecules and a steep adsorption in the region of low relative pressure (P/P_0 = 0.05). Although the water adsorption capacity of kag-MOF-1 is approximately 0.1 g g^{-1} when P/P_0 = 0.05, which is lower than that of AlFFIVE-1-Ni and FeFFIVE-1-Ni, kag-MOF-1 requires less energy in the recycling process because its water adsorption heat is only 60 kJ mol^{-1}. The dynamic breakthrough experiment was conducted at 25 °C and a RH of 75% in a nitrogen flow (8 cm^3 min^{-1}), giving a water retention duration of 1100 min g^{-1}. Changing the gas to a CO_2/N_2 mixture (v/v = 10/90) resulted in a water retention time of 1050 min g^{-1}, which was slightly less than that in the absence of CO_2, indicating that kag-MOF-1 can concomitantly adsorb CO_2 and H_2O. Moreover, kag-MOF-1 exhibited acid resistance and the ability to assimilate H_2S, enabling it to remove H_2O, CO_2, and H_2S from natural gas in one step.[75]

Traditional water-absorbing MOF materials can also be applied in natural gas dehydration. UiO-66-NH_2 and MIL-101 had higher saturated adsorption capacities (0.36 g g^{-1}, 1.41 g g^{-1}) compared to the commercial 3A molecular sieve, alumina and silica. UiO-66-NH_2 (8.3 min g^{-1}) and MIL-101 (18 min g^{-1}) show a longer retention time than commercial adsorbents (<7.5 min g^{-1}) in the dynamic breakthrough experiments carried out with a natural gas flow rate of 200 cm^3 min^{-1} at 75% RH.[6,129]

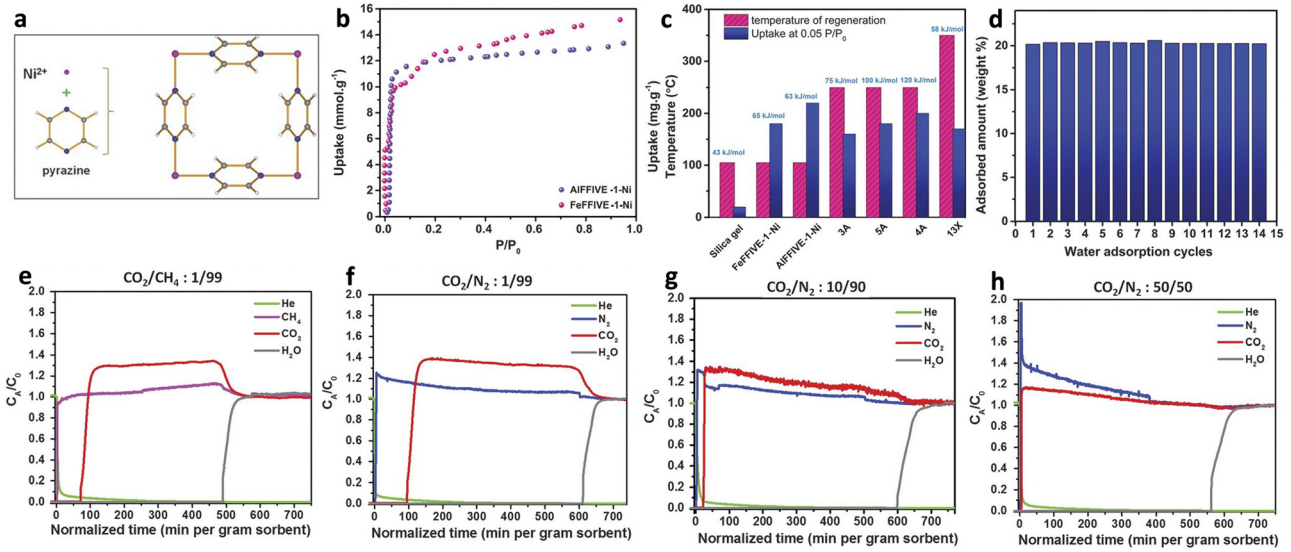

Fig. 18 (a) The repetitive square pattern in the Ni-pyrazine (4,4′) square-grid layer. (b) Water adsorption isotherms of AlFFIVE-1-Ni (violet) and FeFFIVE-1-Ni (pink) at 35 °C. (c) Comparison and relationship between water uptake at P/P_0 = 0.05, heat of sorption, and regeneration temperature of AlFFIVE-1-Ni and FeFFIVE-1-Ni, along with commercial desiccants. (d) Cycles for water absorption uptake of AlFFIVE-1-Ni (adsorption at 25 °C and desorption at 105 °C). (e) Breakthrough test with a humid (75% RH) CO_2/CH_4: 1/99 mixture. (f)–(h) Effect of CO_2 concentration on water breakthrough tests (humid 75% RH). Reproduced with permission from ref. 20. Copyright, 2017, The American Association for the Advancement of Science.

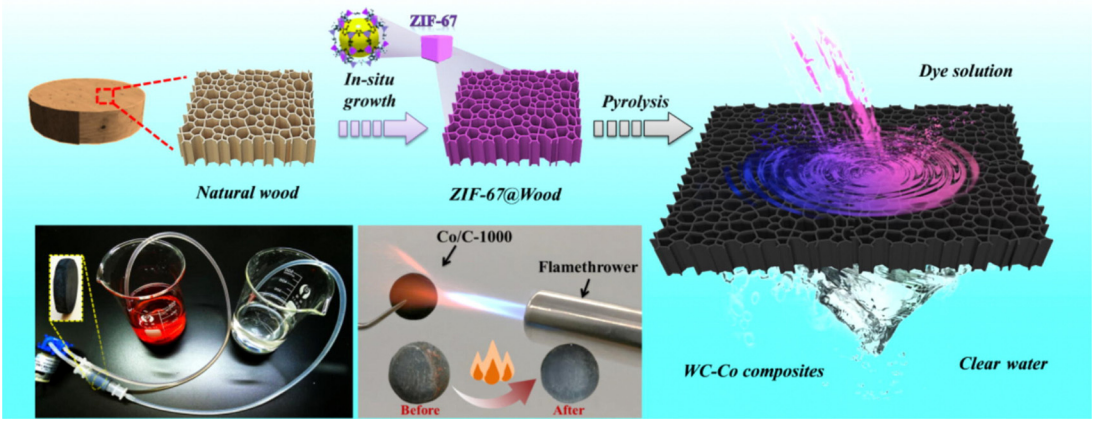

Fig. 19 Schematic diagrams of the preparation of the WC-Co composites for water treatment. Reproduced with permission from ref. 138. Copyright 2022 Elsevier B.V. All rights reserved.

Additionally, MOFs can be utilized for ethanol dehydration in order to produce high-purity ethanol. MAF-45 ($[Cd_4(CH_3COO)_4(H_2dobdim)(H_3dobdim)_2]$, H_4dobdim = 2,6-dihydroxymethyl-benzodiimidazole) and MAF-46 ($[Zn_4(OH)_2(CH_3COO)(Hdobdim)(H_2dobdim)]$) are flexible MOFs featuring high hydrophilicity, consisting of large cavities and minimally sized apertures. MAF-45 possesses a strong affinity to water and shows rigidity without obvious structural changes during water adsorption. For ethanol, the uptake of MAF-45 is low at a low relative pressure, but increases at P/P_0 = 0.6 with 17% volume expansion. For MAF-46 with smaller aperture, the ethanol is hindered during the absorption. Although MAF-46 can gradually expand during the water absorption process, ethanol is still blocked after absorbing water which can occupy the pore apertures acting as a high diffusion barrier for ethanol. This guest-dominated gating adsorption process can avoid the co-adsorption problem effectively. Breakthrough experiments of H_2O/EtOH vapor mixtures (5% and 10% water) were performed, and the two MOFs showed outstanding dehydration performance.[130]

3.5 Water purification

In addition to atmospheric water harvesting, MOFs also can be applied in sea water desalination and water pollution treatment to produce pure water.

The principle of seawater desalination is homologous to harvesting water from the atmosphere. The adsorbent collected the evaporated seawater first and then regenerated it at low temperature, and the desorbed water condensed at the same time. To date, pure water produced by seawater desalination has achieved high-quality distilled water standards.[131] Silica gels have been utilized for desalination, which means MOFs can also be potential candidates for seawater desalination due to the outstanding water absorption property. Simulink simulated seawater desalination and found COP-27(Ni) and aluminum fumarate can produce pure water of 4.3 m^3 per (ton day) at 5 °C and 6 m^3 per (ton day) at 20 °C, respectively.[104] Moreover, aluminum fumarate can produce 6.8 m^3 per (ton day) pure water in practical tests, which is higher than silica gels (5 m^3 per (ton day)).[132]

Furthermore, various metal nanoparticles and fibers have been used for water pollution treatment to dislodge the chlorine,[133,134] heavy metals[135] and dyes.[136] Apart from this, MOFs are widespread in polluted water treatment.[137–140] For instance, Ce(III)-4,4′,4″-((1,3,5-triazine-2,4,6-triyl)tris(azanediyl))-tribenzoic acid-organic framework Ce-H_3tatab-MOFs are available for removing fluoride from water. Under 318 K and pH = 4, the Langmuir adsorption capacity of Ce-H_3tatab-MOFs for F^- can attain 129.7 mg g^{-1} after a series of synthetic modifications.[139] Jiang *et al.* produced WC-CO composites by carbonizing the ZIF-67/wood composite for dye removal (Fig. 19). The adsorption of CR and MB (Congo red (CR) and cationic dye methylene blue (MB)) by the composite was 1117.03 and 805.08 mg g^{-1}, respectively. When the dye concentration reached 1200 mg L^{-1}, 99.98% of dye can be removed by using WC-CO composites.[138]

4. Conclusions and outlook

MOFs have emerged as promising candidates in the field of water absorption because of their abundant adsorption sites and customizable pore structures. In this review, the water absorption characteristics and mechanisms for multiple MOFs were introduced, and the strategies for regulating water absorption properties were elaborated. In the meantime, the applications of water-absorption MOFs in atmospheric water harvesting, indoor humidity control, adsorption-driven heat pump and industrial chemicals dehydration are reviewed. Even though significant progress has been made in water-absorbent MOFs, there are still obstacles that should be overcome to promote the revolution in this field. Here, we proposed some obstacles and possible solutions:

(1) First and foremost, the requests for high water stability of MOFs in specific applications are increasing. The suggested direction for the design and development of new water-absorbing MOFs is to increase the stability of MOFs in

challenging circumstances in order to broaden their usage range under corresponding practical application scenarios.

(2) Although the thermodynamics of water adsorption has been widely investigated, studies on kinetics are still scarce. Note that the pore structure (geometry, size, and chemistry) of the coordination network and morphology of the adsorbent particles, as well as the device construction, can all influence the diffusion of water molecules. Therefore, additional efforts are suggested to optimize water adsorption kinetics. It is proposed that combined with computer simulation, the kinetics of water molecular diffusion should be fully studied on the molecular scale, to design better porous materials.

(3) In recent years, water-absorbing MOFs have demonstrated substantial commercial potential as a result of their extensive spectrum of applications, but the prerequisite is the sustainable large-scale production of MOFs with lower cost and low energy consumption. However, rapid and large-scale synthesis may have an impact on the water absorption performance and structural stability of MOFs, necessitating additional methodological innovations and performance testing to continue development. The development of emerging green synthesis approaches, such as mechanochemistry, chemical vapor deposition and aqueous phase synthesis, will be important ways to reduce costs. Moreover, compositing MOFs with other inexpensive functional adsorbents, such as hydrogels and hygroscopic salts, can also further decrease the costs.

(4) In order to collect enough water to meet the requirements of actual scenarios, not only must the development of adsorbents continue, but also the development of devices. For instance, modifying the closed geometry of passive water collecting devices to increase solar usage or improving the energy utilization of active water harvesting devices is highly desired. Consequently, productivity and stability should be monitored for an extended period in a specific application environment. Meanwhile, other applications, such as indoor humidity maintenance and chemical dehydration, have not yet been fully explored, as a result of which, it is urgent to promptly develop MOF devices for practical applications.

Conflicts of interest

There are no conflicts to declare.

Acknowledgements

We are thankful for the support from the National Natural Science Foundation of China (22071195, 22101231) and The Youth Innovation Team of Shaanxi Universities.

Notes and references

1 P. H. Gleick, Water in crisis: paths to sustainable water use, *Ecol. Appl.*, 1998, **8**, 571–579.
2 M. J. Kalmutzki, C. S. Diercks and O. M. Yaghi, Metal–Organic Frameworks for Water Harvesting from Air, *Adv. Mater.*, 2018, **30**, e1704304.
3 R. S. Schemenauer and P. Cereceda, A proposed standard fog collector for use in high-elevation regions, *J. Appl. Meteorol.*, 1994, **33**, 1313–1322.
4 X. Liu, X. Wang and F. Kapteijn, Water and Metal–Organic Frameworks: From Interaction toward Utilization, *Chem. Rev.*, 2020, **120**, 8303–8377.
5 M. M. Ghiasi, A. Bahadori and S. J. F. Zendehboudi, Estimation of the water content of natural gas dried by solid calcium chloride dehydrator units, *Fuel*, 2014, **117**, 33–42.
6 K. M. C. Santos, T. R. Menezes, M. R. Oliveira, T. S. L. Silva, K. S. Santos, V. A. Barros, D. C. Melo, A. L. Ramos, C. C. Santana, E. Franceschi, C. Dariva, S. M. Egues, G. R. Borges and J. F. De Conto, Natural gas dehydration by adsorption using MOFs and silicas: A review, *Sep. Purif. Technol.*, 2021, **276**, 119409.
7 R. G. AbdulHalim, P. M. Bhatt, Y. Belmabkhout, A. Shkurenko, K. Adil, L. J. Barbour and M. Eddaoudi, A Fine-Tuned Metal–Organic Framework for Autonomous Indoor Moisture Control, *J. Am. Chem. Soc.*, 2017, **139**, 10715–10722.
8 J. Zhang, P. Li, X. Zhang, X. Ma and B. Wang, Aluminum Metal–Organic Frameworks with Photocatalytic Antibacterial Activity for Autonomous Indoor Humidity Control, *ACS Appl. Mater. Interfaces*, 2020, **12**, 46057–46064.
9 M. S. Rahman and T. P. Labuza, *Handbook of food preservation*, CRC Press, 2007, pp. 465–494.
10 A. Karmakar, V. Prabakaran, D. Zhao and K. J. Chua, A review of metal–organic frameworks (MOFs) as energy-efficient desiccants for adsorption driven heat-transformation applications, *Appl. Energy*, 2020, **269**, 115070.
11 E.-P. Ng and S. Mintova, Nanoporous materials with enhanced hydrophilicity and high water sorption capacity, *Microporous Mesoporous Mater.*, 2008, **114**, 1–26.
12 H. Maher, T. H. Rupam, K. A. Rocky, R. Bassiouny and B. B. Saha, Silica gel-MIL 100(Fe) composite adsorbents for ultra-low heat-driven atmospheric water harvester, *Energy*, 2022, **238**, 121741.
13 L. W. Wang, R. Z. Wang and R. G. Oliveira, A review on adsorption working pairs for refrigeration, *Renewable Sustainable Energy Rev.*, 2009, **13**, 518–534.
14 N. Bukovec, P. Bukovec and V. Arbanas, Tg and dsc investigation of $CaCl_2$ $6H_2O$, a phase change material for energy storage, *Thermochim. Acta*, 1989, **148**, 281–288.
15 H. Kim, S. Yang, S. R. Rao, S. Narayanan, E. A. Kapustin, H. Furukawa, A. S. Umans, O. M. Yaghi and E. N. Wang, Water harvesting from air with metal–organic frameworks powered by natural sunlight, *Science*, 2017, **356**, 430–434.
16 F. Fathieh, M. J. Kalmutzki, E. A. Kapustin, P. J. Waller, J. Yang and O. M. Yaghi, Practical water production from desert air, *Sci. Adv.*, 2018, **4**, eaat3198.
17 S. Wang, J. S. Lee, M. Wahiduzzaman, J. Park, M. Muschi, C. Martineau-Corcos, A. Tissot, K. H. Cho, J. Marrot, W. Shepard, G. Maurin, J.-S. Chang and C. Serre, A robust

large-pore zirconium carboxylate metal–organic framework for energy-efficient water-sorption-driven refrigeration, *Nat. Energy*, 2018, **3**, 985–993.

18 D. Lenzen, P. Bendix, H. Reinsch, D. Frohlich, H. Kummer, M. Mollers, P. P. C. Hugenell, R. Glaser, S. Henninger and N. Stock, Scalable Green Synthesis and Full-Scale Test of the Metal–Organic Framework CAU-10-H for Use in Adsorption-Driven Chillers, *Adv. Mater.*, 2018, **30**, 1705869.

19 A. Luna-Triguero, A. Sławek, H. P. Huinink, T. J. H. Vlugt, A. Poursaeidesfahani, J. M. Vicent-Luna and S. Calero, Enhancing the Water Capacity in Zr-Based Metal–Organic Framework for Heat Pump and Atmospheric Water Generator Applications, *ACS Appl. Nano Mater.*, 2019, **2**, 3050–3059.

20 A. Cadiau, Y. Belmabkhout, K. Adil, P. M. Bhatt, R. S. Pillai, A. Shkurenko, C. Martineau-Corcos, G. Maurin and M. Eddaoudi, Hydrolytically stable fluorinated metal–organic frameworks for energy-efficient dehydration, *Science*, 2017, **356**, 731–735.

21 N. X. Zhu, Z. W. Wei, C. X. Chen, X. H. Xiong, Y. Y. Xiong, Z. Zeng, W. Wang, J. J. Jiang, Y. N. Fan and C. Y. Su, High Water Adsorption MOFs with Optimized Pore-Nanospaces for Autonomous Indoor Humidity Control and Pollutants Removal, *Angew. Chem., Int. Ed.*, 2022, **61**, e202112097.

22 S. Kitagawa, R. Kitaura and S. Noro, Functional porous coordination polymers, *Angew. Chem., Int. Ed.*, 2004, **43**, 2334–2375.

23 Y. Duan, Y. Huang, C. Wang, Q. Wang, K. Ge, Z. Lu, H. Wang, J. Duan, J. Bai and W. Jin, Formation and fine-tuning of metal–organic frameworks with carboxylic pincers for the recognition of a C_2H_2 tetramer and highly selective separation of C_2H_2/C_2H_4, *Chem. Sci.*, 2023, **14**, 4605–4611.

24 Q. Dong, Y. Huang, J. Wan, Z. Lu, Z. Wang, C. Gu, J. Duan and J. Bai, Confining Water Nanotubes in a $Cu_{10}O_{13}$-Based Metal–Organic Framework for Propylene/Propane Separation with Record-High Selectivity, *J. Am. Chem. Soc.*, 2023, **145**, 8043–8051.

25 A. U. Czaja, N. Trukhan and U. Muller, Industrial applications of metal–organic frameworks, *Chem. Soc. Rev.*, 2009, **38**, 1284–1293.

26 Q. Dong, Y. Huang, K. Hyeon-Deuk, I. Y. Chang, J. Wan, C. Chen, J. Duan, W. Jin and S. Kitagawa, Shape-and size-dependent kinetic ethylene sieving from a ternary mixture by a trap-and-flow channel crystal, *Adv. Funct. Mater.*, 2022, **32**, 2203745.

27 J. Duan, M. Higuchi, J. Zheng, S.-I. Noro, I. Y. Chang, K. Hyeon-Deuk, S. Mathew, S. Kusaka, E. Sivaniah, R. Matsuda, S. Sakaki and S. Kitagawa, Density Gradation of Open Metal Sites in the Mesospace of Porous Coordination Polymers, *J. Am. Chem. Soc.*, 2017, **139**, 11576–11583.

28 J. R. Li, R. J. Kuppler and H. C. Zhou, Selective gas adsorption and separation in metal–organic frameworks, *Chem. Soc. Rev.*, 2009, **38**, 1477–1504.

29 X. Liu, J. Li, N. Li, B. Li and X. H. Bu, Recent advances on metal–organic frameworks in the conversion of carbon dioxide, *Chin. J. Chem.*, 2021, **39**, 440–462.

30 L. Su, Y. Zhang, X. Qiu, J. Han and Z. Tang, Photocatalytic Carboxylation of Phenyl Halides with CO_2 by Metal–Organic Frameworks Materials, *Chin. J. Chem.*, 2021, **39**, 312–316.

31 S. Sen, N. N. Nair, T. Yamada, H. Kitagawa and P. K. Bharadwaj, High proton conductivity by a metal–organic framework incorporating Zn_8O clusters with aligned imidazolium groups decorating the channels, *J. Am. Chem. Soc.*, 2012, **134**, 19432–19437.

32 Q. Wei, S. Xue, W. Wu, S. Liu, S. Li, C. Zhang and S. Jiang, Plasma Meets MOFs: Synthesis, Modifications, and Functionalities, *Chem. Rec.*, 2023, **23**, e202200263.

33 N. C. Burtch, H. Jasuja and K. S. Walton, Water Stability and Adsorption in Metal–Organic Frameworks, *Chem. Rev.*, 2014, **114**, 10575–10612.

34 A. S. Hall, A. Kondo, K. Maeda and T. E. Mallouk, Microporous brookite-phase titania made by replication of a metal–organic framework, *J. Am. Chem. Soc.*, 2013, **135**, 16276–16279.

35 T. Loiseau, C. Serre, C. Huguenard, G. Fink, F. Taulelle, M. Henry, T. Bataille and G. Ferey, A rationale for the large breathing of the porous aluminum terephthalate (MIL-53) upon hydration, *Chem. – Eur. J.*, 2004, **10**, 1373–1382.

36 A. Vimont, J.-M. Goupil, J.-C. Lavalley, M. Daturi, S. Surblé, C. Serre, F. Millange, G. Férey and N. Audebrand, Investigation of acid sites in a zeotypic giant pores chromium(III) carboxylate, *J. Am. Chem. Soc.*, 2006, **128**, 3218–3227.

37 P. Küsgens, M. Rose, I. Senkovska, H. Fröde, A. Henschel, S. Siegle and S. Kaskel, Characterization of metal–organic frameworks by water adsorption, *Microporous Mesoporous Mater.*, 2009, **120**, 325–330.

38 J.-P. Zhang, A.-X. Zhu, R.-B. Lin, X.-L. Qi and X.-M. Chen, Pore Surface Tailored SOD-Type Metal–Organic Zeolites, *Adv. Mater.*, 2011, **23**, 1268–1271.

39 H. Furukawa, F. Gándara, Y.-B. Zhang, J. Jiang, W. L. Queen, M. R. Hudson and O. M. Yaghi, Water adsorption in porous metal–organic frameworks and related materials, *J. Am. Chem. Soc.*, 2014, **136**, 4369–4381.

40 A. Cadiau, J. S. Lee, D. Damasceno Borges, P. Fabry, T. Devic, M. T. Wharmby, C. Martineau, D. Foucher, F. Taulelle, C. H. Jun, Y. K. Hwang, N. Stock, M. F. De Lange, F. Kapteijn, J. Gascon, G. Maurin, J. S. Chang and C. Serre, Design of hydrophilic metal organic framework water adsorbents for heat reallocation, *Adv. Mater.*, 2015, **27**, 4775–4780.

41 N. Hanikel, X. Pei, S. Chheda, H. Lyu, W. Jeong, J. Sauer, L. Gagliardi and O. M. Yaghi, Evolution of water structures in metal–organic frameworks for improved atmospheric water harvesting, *Science*, 2021, **374**, 454–459.

42 Z. Zheng, N. Hanikel, H. Lyu and O. M. Yaghi, Broadly Tunable Atmospheric Water Harvesting in Multivariate Metal–Organic Frameworks, *J. Am. Chem. Soc.*, 2022, **144**, 22669–22675.

43 Z. Zheng, H. L. Nguyen, N. Hanikel, K. K.-Y. Li, Z. Zhou, T. Ma and O. M. Yaghi, High-yield, green and scalable methods for producing MOF-303 for water harvesting from desert air, *Nat. Protoc.*, 2023, **18**, 136–156.

44 M. Thommes, K. Kaneko, A. V. Neimark, J. P. Olivier, F. Rodriguez-Reinoso, J. Rouquerol and K. S. W. Sing, Physisorption of gases, with special reference to the evaluation of surface area and pore size distribution (IUPAC Technical Report), *Pure Appl. Chem.*, 2015, **87**, 1051–1069.

45 P. D. Dietzel, R. E. Johnsen, R. Blom and H. Fjellvag, Structural changes and coordinatively unsaturated metal atoms on dehydration of honeycomb analogous microporous metal–organic frameworks, *Chem. – Eur. J.*, 2008, **14**, 2389–2397.

46 A. Domán, O. Czakkel, L. Porcar, J. Madarász, E. Geissler and K. László, Role of water molecules in the decomposition of HKUST-1: Evidence from adsorption, thermoanalytical, X-ray and neutron scattering measurements, *Appl. Surf. Sci.*, 2019, **480**, 138–147.

47 H. Reinsch, M. A. van der Veen, B. Gil, B. Marszalek, T. Verbiest, D. de Vos and N. Stock, Structures, Sorption Characteristics, and Nonlinear Optical Properties of a New Series of Highly Stable Aluminum MOFs, *Chem. Mater.*, 2012, **25**, 17–26.

48 J. Canivet, A. Fateeva, Y. Guo, B. Coasne and D. Farrusseng, Water adsorption in MOFs: fundamentals and applications, *Chem. Soc. Rev.*, 2014, **43**, 5594–5617.

49 G. Akiyama, R. Matsuda, H. Sato, A. Hori, M. Takata and S. Kitagawa, Effect of functional groups in MIL-101 on water sorption behavior, *Microporous Mesoporous Mater.*, 2012, **157**, 89–93.

50 A. J. Rieth, S. Yang, E. N. Wang and M. Dinca, Record Atmospheric Fresh Water Capture and Heat Transfer with a Material Operating at the Water Uptake Reversibility Limit, *ACS Cent. Sci.*, 2017, **3**, 668–672.

51 M. Ding, X. Cai and H.-L. Jiang, Improving MOF stability: approaches and applications, *Chem. Sci.*, 2019, **10**, 10209–10230.

52 K. Wang, Y. Li, L. H. Xie, X. Li and J. R. Li, Construction and application of base-stable MOFs: a critical review, *Chem. Soc. Rev.*, 2022, **51**, 6417–6441.

53 J. J. Low, A. I. Benin, P. Jakubczak, J. F. Abrahamian, S. A. Faheem and R. R. Willis, Virtual high throughput screening confirmed experimentally: porous coordination polymer hydration, *J. Am. Chem. Soc.*, 2009, **131**, 15834–15842.

54 T. Y. Luo, S. Park, T. H. Chen, Prerna, R. Patel, X. Li, J. Ilja Siepmann, S. Caratzoulas, Z. Xia and M. Tsapatsis, Simultaneously Enhanced Hydrophilicity and Stability of a Metal–Organic Framework *via* Post-Synthetic Modification for Water Vapor Sorption/Desorption, *Angew. Chem., Int. Ed.*, 2022, **61**, e202209034.

55 H. Xu, Y. Wu, L. Yang, Y. Rao, J. Wang, S. Peng and Q. Li, Water-Harvesting Metal–Organic Frameworks with Gigantic Al(24) Units and their Deconstruction into Molecular Clusters, *Angew. Chem., Int. Ed.*, 2023, **62**, e202217864.

56 F. Jeremias, A. Khutia, S. K. Henninger and C. Janiak, MIL-100(Al, Fe) as water adsorbents for heat transformation purposes—a promising application, *J. Mater. Chem. A*, 2012, **22**, 10148–10151.

57 D. D. Zhou, P. Chen, C. Wang, S. S. Wang, Y. Du, H. Yan, Z. M. Ye, C. T. He, R. K. Huang, Z. W. Mo, N. Y. Huang and J. P. Zhang, Intermediate-sized molecular sieving of styrene from larger and smaller analogues, *Nat. Mater.*, 2019, **18**, 994–998.

58 F. Jeremias, D. Fröhlich, C. Janiak and S. K. Henninger, Advancement of sorption-based heat transformation by a metal coating of highly-stable, hydrophilic aluminium fumarate MOF, *RSC Adv.*, 2014, **4**, 24073–24082.

59 G. E. Cmarik, M. Kim, S. M. Cohen and K. S. Walton, Tuning the adsorption properties of UiO-66 *via* ligand functionalization, *Langmuir*, 2012, **28**, 15606–15613.

60 F.-F. Lu, X.-W. Gu, E. Wu, B. Li and G. Qian, Systematic evaluation of water adsorption in isoreticular UiO-type metal–organic frameworks, *J. Mater. Chem. A*, 2023, **11**, 1246–1255.

61 V. Bon, I. Senkovska, J. D. Evans, M. Wöllner, M. Hölzel and S. Kaskel, Insights into the water adsorption mechanism in the chemically stable zirconium-based MOF DUT-67 – a prospective material for adsorption-driven heat transformations, *J. Mater. Chem. A*, 2019, **7**, 12681–12690.

62 D. Frohlich, S. K. Henninger and C. Janiak, Multicycle water vapour stability of microporous breathing MOF aluminium isophthalate CAU-10-H, *Dalton Trans.*, 2014, **43**, 15300–15304.

63 S.-N. Kim, J. Kim, H.-Y. Kim, H.-Y. Cho and W.-S. Ahn, Adsorption/catalytic properties of MIL-125 and NH2-MIL-125, *Catal. Today*, 2013, **204**, 85–93.

64 A. Shigematsu, T. Yamada and H. Kitagawa, Wide control of proton conductivity in porous coordination polymers, *J. Am. Chem. Soc.*, 2011, **133**, 2034–2036.

65 N. Reimer, B. Gil, B. Marszalek and N. Stock, Thermal post-synthetic modification of Al-MIL-53–COOH: systematic investigation of the decarboxylation and condensation reaction, *CrystEngComm*, 2012, **14**, 4119–4125.

66 Y. Han, P. Das, Y. He, D. C. Sorescu, K. D. Jordan and N. L. Rosi, Crystallographic Mapping and Tuning of Water Adsorption in Metal–Organic Frameworks Featuring Distinct Open Metal Sites, *J. Am. Chem. Soc.*, 2022, **144**, 19567–19575.

67 G. Akiyama, R. Matsuda and S. Kitagawa, Highly porous and stable coordination polymers as water sorption materials, *Chem. Lett.*, 2010, **39**, 360–361.

68 N. Ko, P. G. Choi, J. Hong, M. Yeo, S. Sung, K. E. Cordova, H. J. Park, J. K. Yang and J. Kim, Tailoring the water adsorption properties of MIL-101 metal–organic frameworks by partial functionalization, *J. Mater. Chem. A*, 2015, **3**, 2057–2064.

69 A. J. Rieth, A. M. Wright, G. Skorupskii, J. L. Mancuso, C. H. Hendon and M. Dinca, Record-Setting Sorbents for Reversible Water Uptake by Systematic Anion Exchanges in Metal–Organic Frameworks, *J. Am. Chem. Soc.*, 2019, **141**, 13858–13866.

70 S. M. Towsif Abtab, D. Alezi, P. M. Bhatt, A. Shkurenko, Y. Belmabkhout, H. Aggarwal, Ł. J. Weseliński, N. Alsadun, U. Samin, M. N. Hedhili and M. Eddaoudi, Reticular

Chemistry in Action: A Hydrolytically Stable MOF Capturing Twice Its Weight in Adsorbed Water, *Chem*, 2018, **4**, 94–105.

71 D. Ma, P. Li, X. Duan, J. Li, P. Shao, Z. Lang, L. Bao, Y. Zhang, Z. Lin and B. Wang, A Hydrolytically Stable Vanadium(IV) Metal–Organic Framework with Photocatalytic Bacteriostatic Activity for Autonomous Indoor Humidity Control, *Angew. Chem., Int. Ed.*, 2020, **59**, 3905–3909.

72 Z. Chen, P. Li, X. Zhang, P. Li, M. C. Wasson, T. Islamoglu, J. F. Stoddart and O. K. Farha, Reticular Access to Highly Porous acs-MOFs with Rigid Trigonal Prismatic Linkers for Water Sorption, *J. Am. Chem. Soc.*, 2019, **141**, 2900–2905.

73 B. Li, F. F. Lu, X. W. Gu, K. Shao, E. Wu and G. Qian, Immobilization of Lewis Basic Nitrogen Sites into a Chemically Stable Metal–Organic Framework for Benchmark Water-Sorption-Driven Heat Allocations, *Adv. Sci.*, 2022, **9**, e2105556.

74 K. H. Cho, D. D. Borges, U. H. Lee, J. S. Lee, J. W. Yoon, S. J. Cho, J. Park, W. Lombardo, D. Moon, A. Sapienza, G. Maurin and J. S. Chang, Rational design of a robust aluminum metal–organic framework for multi-purpose water-sorption-driven heat allocations, *Nat. Commun.*, 2020, **11**, 5112.

75 M. I. H. Mohideen, R. S. Pillai, K. Adil, P. M. Bhatt, Y. Belmabkhout, A. Shkurenko, G. Maurin and M. Eddaoudi, A Fine-Tuned MOF for Gas and Vapor Separation: A Multipurpose Adsorbent for Acid Gas Removal, Dehydration, and BTX Sieving, *Chem*, 2017, **3**, 822–833.

76 Q. M. Wang, D. Shen, M. Bülow, M. L. Lau, S. Deng, F. R. Fitch, N. O. Lemcoff and J. Semanscin, Metallo-organic molecular sieve for gas separation and purification, *Microporous Mesoporous Mater.*, 2002, **55**, 217–230.

77 P. M. Schoenecker, C. G. Carson, H. Jasuja, C. J. J. Flemming and K. S. Walton, Effect of Water Adsorption on Retention of Structure and Surface Area of Metal–Organic Frameworks, *Ind. Eng. Chem. Res.*, 2012, **51**, 6513–6519.

78 S. K. Henninger, F. Jeremias, H. Kummer and C. Janiak, MOFs for Use in Adsorption Heat Pump Processes, *Eur. J. Inorg. Chem.*, 2011, 2625–2634.

79 J. Canivet, J. Bonnefoy, C. Daniel, A. Legrand, B. Coasne and D. Farrusseng, Structure–property relationships of water adsorption in metal–organic frameworks, *New J. Chem.*, 2014, **38**, 3102–3111.

80 F.-X. Coudert, A. Boutin, A. H. Fuchs and A. V. Neimark, Adsorption Deformation and Structural Transitions in Metal–Organic Frameworks: From the Unit Cell to the Crystal, *J. Phys. Chem. Lett.*, 2013, **4**, 3198–3205.

81 M. I. Hossain and T. G. Glover, Kinetics of Water Adsorption in UiO-66 MOF, *Ind. Eng. Chem. Res.*, 2019, **58**, 10550–10558.

82 D. Fröhlich, E. Pantatosaki, P. D. Kolokathis, K. Markey, H. Reinsch, M. Baumgartner, M. A. van der Veen, D. E. De Vos, N. Stock, G. K. Papadopoulos, S. K. Henninger and C. Janiak, Water adsorption behaviour of CAU-10-H: a thorough investigation of its structure–property relationships, *J. Mater. Chem. A*, 2016, **4**, 11859–11869.

83 M. F. de Lange, T. Zeng, T. J. H. Vlugt, J. Gascon and F. Kapteijn, Manufacture of dense CAU-10-H coatings for application in adsorption driven heat pumps: optimization and characterization, *CrystEngComm*, 2015, **17**, 5911–5920.

84 W. Liu, E. Wu, B. Yu, Z. Liu, K. Wang, D. Qi, B. Li and J. Jiang, Reticular Synthesis of Metal–Organic Frameworks by 8-Connected Quadrangular Prism Ligands for Water Harvesting, *Angew. Chem., Int. Ed.*, 2023, **62**, e202305144.

85 P. L. Llewellyn, S. Bourrelly, C. Serre, A. Vimont, M. Daturi, L. Hamon, G. De Weireld, J.-S. Chang, D.-Y. Hong and Y. Kyu, Hwang, High uptakes of CO2 and CH4 in mesoporous metal–organic frameworks mil-100 and mil-101, *Langmuir*, 2008, **24**, 7245–7250.

86 G. Férey, C. Mellot-Draznieks, C. Serre and F. Millange, Crystallized frameworks with giant pores: are there limits to the possible?, *Acc. Chem. Res.*, 2005, **38**, 217–225.

87 J. Ehrenmann, S. K. Henninger and C. Janiak, Water Adsorption Characteristics of MIL-101 for Heat-Transformation Applications of MOFs, *Eur. J. Inorg. Chem.*, 2010, 471–474.

88 Y. Wang, N. Y. Huang, J. Q. Shen, P. Q. Liao, X. M. Chen and J. P. Zhang, Hydroxide Ligands Cooperate with Catalytic Centers in Metal–Organic Frameworks for Efficient Photocatalytic CO(2) Reduction, *J. Am. Chem. Soc.*, 2018, **140**, 38–41.

89 A. J. Rieth, K. M. Hunter, M. Dinca and F. Paesani, Hydrogen bonding structure of confined water templated by a metal–organic framework with open metal sites, *Nat. Commun.*, 2019, **10**, 4771.

90 D. Damasceno Borges, G. Maurin and D. S. Galvão, Design of Porous Metal–Organic Frameworks for Adsorption Driven Thermal Batteries, *MRS Adv.*, 2017, **2**, 519–524.

91 A. Permyakova, O. Skrylnyk, E. Courbon, M. Affram, S. Wang, U. H. Lee, A. H. Valekar, F. Nouar, G. Mouchaham, T. Devic, G. De Weireld, J. S. Chang, N. Steunou, M. Frere and C. Serre, Synthesis Optimization, Shaping, and Heat Reallocation Evaluation of the Hydrophilic Metal–Organic Framework MIL-160(Al), *ChemSusChem*, 2017, **10**, 1419–1426.

92 N. C. Burtch and K. S. Walton, Modulating adsorption and stability properties in pillared metal–organic frameworks: a model system for understanding ligand effects, *Acc. Chem. Res.*, 2015, **48**, 2850–2857.

93 Q. Dong, X. Zhang, S. Liu, R. B. Lin, Y. Guo, Y. Ma, A. Yonezu, R. Krishna, G. Liu, J. Duan, R. Matsuda, W. Jin and B. Chen, Tuning Gate-Opening of a Flexible Metal–Organic Framework for Ternary Gas Sieving Separation, *Angew. Chem., Int. Ed.*, 2020, **59**, 22756–22762.

94 Y. Huang, J. Wan, T. Pan, K. Ge, Y. Guo, J. Duan, J. Bai, W. Jin and S. Kitagawa, Delicate Softness in a Temperature-Responsive Porous Crystal for Accelerated Sieving of Propylene/Propane, *J. Am. Chem. Soc.*, 2023, **145**, 24425–24432.

95 J. Arinez-Soriano, J. Albalad, C. Vila-Parrondo, J. Perez-Carvajal, S. Rodriguez-Hermida, A. Cabeza, J. Juanhuix, I. Imaz and D. Maspoch, Single-crystal and humidity-controlled powder diffraction study of the breathing effect

in a metal–organic framework upon water adsorption/desorption, *Chem. Commun.*, 2016, **52**, 7229–7232.

96 S. Bourrelly, B. Moulin, A. Rivera, G. Maurin, S. Devautour-Vinot, C. Serre, T. Devic, P. Horcajada, A. Vimont and G. Clet, Explanation of the adsorption of polar vapors in the highly flexible metal organic framework MIL-53 (Cr), *J. Am. Chem. Soc.*, 2010, **132**, 9488–9498.

97 F.-X. Coudert, A. U. Ortiz, V. Haigis, D. Bousquet, A. H. Fuchs, A. Ballandras, G. Weber, I. Bezverkhyy, N. Geoffroy, J.-P. Bellat, G. Ortiz, G. Chaplais, J. Patarin and A. Boutin, Water Adsorption in Flexible Gallium-Based MIL-53 Metal–Organic Framework, *J. Phys. Chem. C*, 2014, **118**, 5397–5405.

98 S. Devautour-Vinot, G. Maurin, F. Henn, C. Serre and G. Ferey, Water and ethanol desorption in the flexible metal organic frameworks, MIL-53 (Cr, Fe), investigated by complex impedance spectroscopy and density functional theory calculations, *Phys. Chem. Chem. Phys.*, 2010, **12**, 12478–12485.

99 S. Biswas, T. Ahnfeldt and N. Stock, New functionalized flexible Al-MIL-53-X (X = –Cl, –Br, $-CH_3$, $-NO_2$, $-(OH)_2$) solids: syntheses, characterization, sorption, and breathing behavior, *Inorg. Chem.*, 2011, **50**, 9518–9526.

100 M. Shivanna, A. A. Bezrukov, V. Gascón-Pérez, K.-I. Otake, S. Sanda, D. J. O'Hearn, Q.-Y. Yang, S. Kitagawa and M. Zaworotko, Flexible coordination network exhibiting water vapor-induced reversible switching between closed and open phases, *ACS Appl. Mater. Interfaces*, 2022, **14**, 39560–39566.

101 A. Subanbekova, V. I. Nikolayenko, A. A. Bezrukov, D. Sensharma, N. Kumar, D. J. O'Hearn, V. Bon, S.-Q. Wang, K. Koupepidou, S. Darwish, S. Kaskel and M. J. Zaworotko, Water vapour and gas induced phase transformations in an 8-fold interpenetrated diamondoid metal–organic framework, *J. Mater. Chem. A*, 2023, **11**, 9691–9699.

102 M. M. Mekonnen and A. Y. Hoekstra, Four billion people facing severe water scarcity, *Sci. Adv.*, 2016, **2**, e1500323.

103 J. Wang, L. Hua, C. Li and R. Wang, Atmospheric water harvesting: critical metrics and challenges, *Energy Environ. Sci.*, 2022, **15**, 4867–4871.

104 E. Elsayed, R. Al-Dadah, S. Mahmoud, P. A. Anderson, A. Elsayed and P. G. Youssef, CPO-27(Ni), aluminium fumarate and MIL-101(Cr) MOF materials for adsorption water desalination, *Desalination*, 2017, **406**, 25–36.

105 W. Xu and O. M. Yaghi, Metal–Organic Frameworks for Water Harvesting from Air, Anywhere, Anytime, *ACS Cent. Sci.*, 2020, **6**, 1348–1354.

106 N. Hanikel, M. S. Prevot and O. M. Yaghi, MOF water harvesters, *Nat. Nanotechnol.*, 2020, **15**, 348–355.

107 R. D. Stelmach and T. Clasen, Household water quantity and health: a systematic review, *Int. J. Environ. Res. Public Health*, 2015, **12**, 5954–5974.

108 N. Hanikel, M. S. Prevot, F. Fathieh, E. A. Kapustin, H. Lyu, H. Wang, N. J. Diercks, T. G. Glover and O. M. Yaghi, Rapid Cycling and Exceptional Yield in a Metal–Organic Framework Water Harvester, *ACS Cent. Sci.*, 2019, **5**, 1699–1706.

109 H. A. Almassad, R. I. Abaza, L. Siwwan, B. Al-Maythalony and K. E. Cordova, Environmentally adaptive MOF-based device enables continuous self-optimizing atmospheric water harvesting, *Nat. Commun.*, 2022, **13**, 4873.

110 Z. Shao, Y.-C. Tang, H. Lv, Z.-S. Wang, P. Poredoš, Y. Feng, R. Sun, X. Feng, Z. Chen, Z. Gao, D.-D. Zhou, J.-P. Zhang and R. Wang, High-performance solar-driven MOF AWH device with ultra-dense integrated modular design and reflux synthesis of Ni_2Cl_2 (BTDD), *Device*, 2023, **1**, 100058.

111 Y. Feng, T. Ge, B. Chen, G. Zhan and R. Wang, A regulation strategy of sorbent stepwise position for boosting atmospheric water harvesting in arid area, *Cell Rep. Phys. Sci.*, 2021, **2**, 100561.

112 J. Wu, Z. Sui, X. Du, Y. Zhang and T. Ma, A Study on the Improvement of the Photothermal Characteristics of the Adsorbent for Sorption-Based Atmospheric Water Harvesting Driven by Solar, *Coatings*, 2023, **13**, 154.

113 G. Yilmaz, F. Meng, W. Lu, J. Abed, C. Peh, M. Gao, E. Sargent and G. Ho, Autonomous atmospheric water seeping MOF matrix, *Sci. Adv.*, 2020, **6**, eabc8605.

114 A. Persily, Challenges in developing ventilation and indoor air quality standards: The story of ASHRAE Standard 62, *Build. Environ.*, 2015, **91**, 61–69.

115 A. V. Arundel, E. M. Sterling, J. H. Biggin and T. D. Sterling, Indirect health effects of relative humidity in indoor environments, *Environ. Health Perspect.*, 1986, **65**, 351–361.

116 M. Isaac and D. P. Van Vuuren, Modeling global residential sector energy demand for heating and air conditioning in the context of climate change, *Energy Policy*, 2009, **37**, 507–521.

117 J. B. DeCoste, G. W. Peterson, B. J. Schindler, K. L. Killops, M. A. Browe and J. J. Mahle, The effect of water adsorption on the structure of the carboxylate containing metal–organic frameworks Cu-BTC, Mg-MOF-74, and UiO-66, *J. Mater. Chem. A*, 2013, **1**, 11922.

118 S. B. Riffat and X. Ma, Improving the coefficient of performance of thermoelectric cooling systems: a review, *Int. J. Energy Res.*, 2004, **28**, 753–768.

119 F. Jeremias, D. Fröhlich, C. Janiak and S. K. Henninger, Water and methanol adsorption on MOFs for cycling heat transformation processes, *New J. Chem.*, 2014, **38**, 1846–1852.

120 S. K. Henninger, H. A. Habib and C. Janiak, MOFs as adsorbents for low temperature heating and cooling applications, *J. Am. Chem. Soc.*, 2009, **131**, 2776–2777.

121 F. Xu, Z. F. Bian, T. S. Ge, Y. J. Dai, C. H. Wang and S. Kawi, Analysis on solar energy powered cooling system based on desiccant coated heat exchanger using metal–organic framework, *Energy*, 2019, **177**, 211–221.

122 H. W. B. Teo, A. Chakraborty, Y. Kitagawa and S. Kayal, Experimental study of isotherms and kinetics for adsorption of water on Aluminium Fumarate, *Int. J. Heat Mass Transfer*, 2017, **114**, 621–627.

123 H. Kummer, F. Jeremias, A. Warlo, G. Füldner, D. Fröhlich, C. Janiak, R. Gläser and S. K. Henninger, A Functional Full-Scale Heat Exchanger Coated with Aluminum Fumarate Metal–Organic Framework for Adsorption Heat Transformation, *Ind. Eng. Chem. Res.*, 2017, **56**, 8393–8398.

124 M. F. de Lange, K. J. Verouden, T. J. Vlugt, J. Gascon and F. Kapteijn, Adsorption-Driven Heat Pumps: The Potential of Metal–Organic Frameworks, *Chem. Rev.*, 2015, **115**, 12205–12250.
125 B. N. Truong, D. D. Borges, J. Park, J. S. Lee, D. Jo, J. S. Chang, S. J. Cho, G. Maurin, K. H. Cho and U. H. Lee, Tuning Hydrophilicity of Aluminum MOFs by a Mixed-Linker Strategy for Enhanced Performance in Water Adsorption-Driven Heat Allocation Application, *Adv. Sci.*, 2023, **10**, 2301311.
126 H. Liu, Y. He, J. Jiao, D. Bai, D. L. Chen, R. Krishna and B. Chen, A Porous Zirconium-Based Metal–Organic Framework with the Potential for the Separation of Butene Isomers, *Chem. – Eur. J.*, 2016, **22**, 14988–14997.
127 M. Netusil and P. Ditl, Comparison of three methods for natural gas dehydration, *J. Nat. Gas Chem.*, 2011, **20**, 471–476.
128 P. Gandhidasan, A. A. Al-Farayedhi and A. A. Al-Mubarak, Dehydration of natural gas using solid desiccants, *Energy*, 2001, **26**, 855–868.
129 R. Mesgarian, A. Heidarinasab, A. Rashidi and Y. Zamani, High Performance MIL-101 Nanoadsorbent for the Natural Gas Dehydration, *J. Nanostruct.*, 2022, **12**, 983–998.
130 Y. C. Tang, Z. S. Wang, H. Yi, M. Y. Zhou, D. D. Zhou, J. P. Zhang and X. M. Chen, Water-Stable Metal Azolate Frameworks Showing Interesting Flexibilities for Highly Effective Bioethanol Dehydration, *Angew. Chem., Int. Ed.*, 2023, **62**, e202303374.
131 Y.-D. Kim, K. Thu, M. E. Masry and K. C. Ng, Water quality assessment of solar-assisted adsorption desalination cycle, *Desalination*, 2014, **344**, 144–151.
132 E. Elsayed, R. Al-Dadah, S. Mahmoud, P. Anderson and A. Elsayed, Experimental testing of aluminium fumarate MOF for adsorption desalination, *Desalination*, 2020, **475**, 114170.
133 S. Jian, Y. Cheng, X. Ma, H. Guo, J. Hu, K. Zhang, S. Jiang, W. Yang and G. Duan, Excellent fluoride removal performance by electrospun La–Mn bimetal oxide nanofibers, *New J. Chem.*, 2022, **46**, 490–497.
134 S. Jian, Y. Chen, F. Shi, Y. Liu, W. Jiang, J. Hu, X. Han, S. Jiang and W. Yang, Template-Free Synthesis of Magnetic La-Mn-Fe Tri-Metal Oxide Nanofibers for Efficient Fluoride Remediation: Kinetics, Isotherms, Thermodynamics and Reusability, *Polymers*, 2022, **14**, 5417.
135 W. Yang, Y. Wang, Q. Wang, J. Wu, G. Duan, W. Xu and S. Jian, Magnetically separable and recyclable Fe_3O_4@PDA covalent grafted by l-cysteine core-shell nanoparticles toward efficient removal of Pb^{2+}, *Vacuum*, 2021, **189**, 110229.
136 S. Jian, Z. Tian, K. Zhang, G. Duan, W. Yang and S. Jiang, Hydrothermal Synthesis of Ce-doped ZnO Heterojunction Supported on Carbon Nanofibers with High Visible Light Photocatalytic Activity, *Chem. Res. Chin. Univ.*, 2021, **37**, 565–570.
137 J. Wang, Y. Sun, X. Zhao, L. Chen, S. Peng, C. Ma, G. Duan, Z. Liu, H. Wang, Y. Yuan and N. Wang, A poly(amidoxime)-modified MOF macroporous membrane for high-efficient uranium extraction from seawater, *e-Polym.*, 2022, **22**, 399–410.
138 X. Ma, S. Zhao, Z. Tian, G. Duan, H. Pan, Y. Yue, S. Li, S. Jian, W. Yang, K. Liu, S. He and S. Jiang, MOFs meet wood: Reusable magnetic hydrophilic composites toward efficient water treatment with super-high dye adsorption capacity at high dye concentration, *Chem. Eng. J.*, 2022, **446**, 136851.
139 J. Song, W. Yang, X. Han, S. Jiang, C. Zhang, W. Pan, S. Jian and J. Hu, Performance of Rod-Shaped Ce Metal–Organic Frameworks for Defluoridation, *Molecules*, 2023, **28**, 3492.
140 J. Hu, J. Song, X. Han, Q. Wen, W. Yang, W. Pan, S. Jian and S. Jiang, Fabrication of Ce-La-MOFs for defluoridation in aquatic systems: A kinetics, thermodynamics and mechanisms study, *Sep. Purif. Technol.*, 2023, **314**, 123562.

